ADVANCED MATERIALS
www.advmat.de

Recent Progress in Strain Engineering on Van der Waals 2D Materials: Tunable Electrical, Electrochemical, Magnetic, and Optical Properties

Yaping Qi, Mohammad A. Sadi, Dan Hu, Ming Zheng, Zhenping Wu, Yucheng Jiang,* and Yong P. Chen**

Strain engineering is a promising way to tune the electrical, electrochemical, magnetic, and optical properties of 2D materials, with the potential to achieve high-performance 2D-material-based devices ultimately. This review discusses the experimental and theoretical results from recent advances in the strain engineering of 2D materials. Some novel methods to induce strain are summarized and then the tunable electrical and optical/optoelectronic properties of 2D materials via strain engineering are highlighted, including particularly the previously less-discussed strain tuning of superconducting, magnetic, and electrochemical properties. Also, future perspectives of strain engineering are given for its potential applications in functional devices. The state of the survey presents the ever-increasing advantages and popularity of strain engineering for tuning properties of 2D materials. Suggestions and insights for further research and applications in optical, electronic, and spintronic devices are provided.

1. Introduction

2D materials are atomically thin layers with high flexibility and strain sensitivity.[1–3] Phonons and electrons in 2D materials are limited in the planar dimensions, resulting in many distinct and outstanding properties compared to their 3D bulk counterparts.[2] Therefore, 2D materials are ideal for flexible optoelectronics and have the potential to be used in the next-generation ultrathin electronic and optoelectronic devices.[1] The concept of 2D materials was first realized when graphene was found in 2004.[4] Graphene has attracted extensive attention for its excellent electrical, optical, and mechanical properties.[4–6] They have been investigated for various technological applications, including spintronics, sensors, optoelectronics, supercapacitors, and solar cells, etc.[5,7] Besides graphene, other 2D materials, such as h-BN, phosphorene, silicene, germanene, and transition metal dichalcogenides (molybdenum disulfide (MoS_2), molybdenum diselenide ($MoSe_2$), tungsten disulfide (WS_2), and tungsten diselenide (WSe_2), etc.), have been studied extensively in recent years.[1,8–11] The thickness of single-layer 2D materials is usually on the order or less than 1 nm. At the same time, their lateral sizes could reach much larger size (from microns to even inches), and 2D materials can be transferred to different substrates before subsequent processing or follow-up measurements for characterizations or device applications.

Y. Qi, D. Hu, Y. P. Chen
Department of Engineering Science, Faculty of Innovation Engineering
Macau University of Science and Technology
Av. Wai Long, Macao SAR, China
E-mail: ypqi@must.edu.mo

M. A. Sadi, Y. P. Chen
Elmore Family School of Electrical and Computer Engineering
Purdue University
West Lafayette, IN 47907, USA
E-mail: yongchen@purdue.edu

M. Zheng
School of Materials Science and Physics
China University of Mining and Technology
Xuzhou 221116, China

The ORCID identification number(s) for the author(s) of this article can be found under https://doi.org/10.1002/adma.202205714.

DOI: 10.1002/adma.202205714

Z. Wu
State Key Laboratory of Information Photonics and Optical Communications & School of Science
Beijing University of Posts and Telecommunications
Beijing 100876, China

Y. Jiang
Jiangsu Key Laboratory of Micro and Nano Heat Fluid Flow Technology and Energy Application
School of Physical Science and Technology
Suzhou University of Science and Technology
Suzhou, Jiangsu 215009, P. R. China
E-mail: jyc@usts.edu.cn

Y. P. Chen
Department of Physics and Astronomy and Birck Nanotechnology Center and Purdue Quantum Science and Engineering Institute
Purdue University
West Lafayette, IN 47907, USA

Y. P. Chen
Institute of Physics and Astronomy and Villum Center for Hybrid Quantum Materials and Devices
Aarhus University
Aarhus-C 8000, Denmark

Strain engineering is an effective and promising way to manipulate the electrical, magnetic, and optical properties of 2D materials. The multiple tunable functionalities (electrical, magnetic, optical, and mechanical) and their intercouplings in 2D materials provide rich opportunities to design innovative materials or composites with broad applications in electromechanical devices and sensors, etc. Given the promising application of strain engineering of 2D materials, there have emerged increasing number of research studies and review papers on this topic.[12–33] For example, Guinea[29] reviewed strain engineering on the electronic properties of graphene. Bissett et al.[30] summarized recent advances in strain engineering using Raman spectroscopy and electrical transport and the effect of strain on the chemical function of graphene. Roldán et al.[31] discussed the progress of strain engineering to control the electronic and optical properties of semiconducting 2D crystals. Si et al.[32] examined the effect of strain in graphene on the electronic structure, Raman spectra, the electron–phonon coupling, pseudo magnetic fields, and the potential applications of strain engineering in the self-assembly of foreign atoms on the surface of graphene. Deng et al.[2] introduced the structure and mechanical properties of different kinds of 2D nanomaterials, summarized the methods to induce strain, and reviewed various modified properties caused by strain engineering, followed by a discussion about future perspectives. Dai et al.[1] summarized new opportunities and challenges focusing on the interface properties. Du et al.[3] outlined the recent progress of strain engineering on the flexible optoelectronics of 2D materials and discussed the current challenges in this area. Blundo et al.[33] have comprehensively summarized strain-tuned electronic, optical, and vibrational properties of 2D crystals.

Despite the fair number of reviews already published on this topic as cited above,[12–33] we present an updated review motivated by the rapid pace of advancement in this field and a number of more recent and important new developments, ranging from new experimental methods to new or less reviewed properties (e.g., magnetic, superconducting, electrochemical) explored in strain engineering. In this review, we summarized and discussed recently reported new methods to induce strain, updated the latest developments on the modification of electrical, magnetic, and optical properties of 2D materials by strain engineering, and presented future perspectives.

2. Novel Methodology to Induce Strain

Different methods have been previously applied to induce or engineer strain in 2D materials, through intrinsic ripples, mechanical exfoliation, epitaxial growth, thermal expansion mismatch, strain relaxation and critical thickness in heterostructures, chemical doping and absorption, deformation of flexible substrates, substrate surface topography modification, piezoelectric substrate actuation, as well as pressurized blisters, blown-bubble, and tip indentation. The advantages and disadvantages of all these methods have been summarized by Deng et al.[2] previously. Some newly emerging or optimized approaches to induce strain in 2D materials are updated and discussed herein.

2.1. Polymer Encapsulation

One limitation in many previous methods for straining and manipulating 2D materials is weak van der Waals (vdW) interaction and severe slippage between the substrate and 2D material. Recently, Li et al.[34] developed a simple method to efficiently modulate the strain of 2D materials by polymer encapsulation (**Figure 1**a,b). Using a spin-coating approach, the monolayer 2D material (MoS_2) was encapsulated in a flexible PVA substrate (Figure 1a,b). The mechanical strain could easily be transferred with negligible decoupling or slippage because of the strong interaction between 2D material and spin-coated PVA. When the uniaxial strain was applied to monolayer MoS_2, a modulation rate (≈136 meV per %) and a bandgap modulation (≈300 meV) were observed. The modulation rate and bandgap modulation are two times of the results previously obtained.[34] It is worth noting that this simple method is also applicable to other 2D materials, including WS_2 or WSe_2, for increased bandgap modulation.[34] However, the spin-coating encapsulation approach can only provide strong interaction primarily between one layer of 2D material and the PVA substrate. At the same time, vdW heterostructures would remain bonded by weak vdW interaction, and the interlayer transfer of strain may mainly determine the overall device strain property.[34] Therefore, this method should be further optimized to work well to introduce strain on vdW heterostructures.

2.2. Local Strain Application

Some available approaches for strain induction are not ideal because they need complicated growth steps or macroscopic mechanical stresses. Furthermore, these methods cannot manage the strain locally at individual flake level and on a large scale to many individual devices on a single chip in engineering 2D material devices. Several studies reported the application of local strains.[35,36] For example, Mikael et al.[35] demonstrated the application of the nitride stressor layer to cause triaxial compressive stress in bilayer graphene. Colangelo et al.[36] used micrometric polymeric actuators to control local deformation in graphene. Peña et al.[37] reported a new method to induce compressive and tensile strain into MoS_2 through depositing stressed thin films to encapsulate exfoliated flakes. This technique can be used to directly engineer MoS_2 strain magnitude by modifying deposited thin film stress, allowing the application of different strains on a flake-to-flake level. After depositing a tensile thin-film stressor onto MoS_2, the stressor would contract and result in compressive strain transferred to the MoS_2 layers. Due to substrate adhesion, when MoS_2 was grown on conventional substrates such as MgO or SiO_2, only limited strain was transferred to monolayers.[37] To avoid this limitation, Peña et al. tested stressors on vdW heterostructures composed of monolayer (1L) MoS_2 on hexagonal boron nitride (h-BN). This method allows 0.85% of strain to be applied to the monolayer MoS_2 with a corresponding bandgap change (75 meV) induced by strain. It is expected that strain could be engineered to be higher if higher stressed thin films were used.[37] This study presented a different mechanism where strain is transferred using evaporated stressed polycrystalline thin

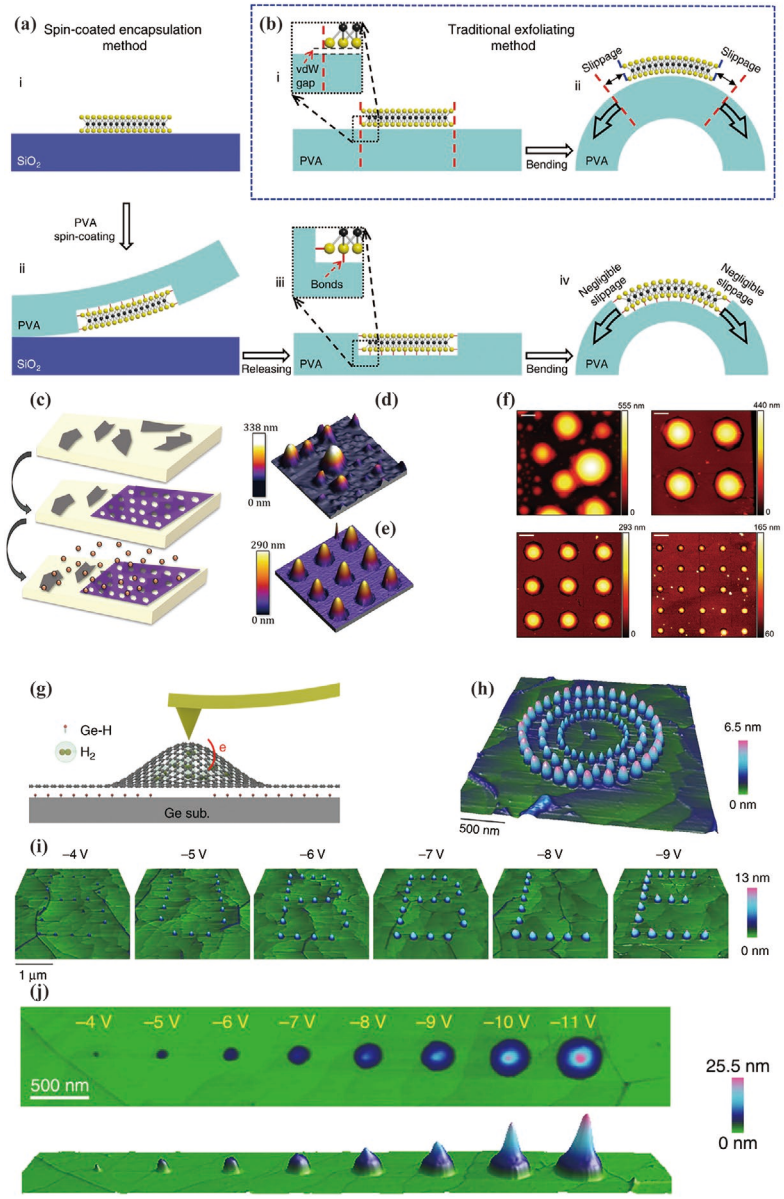

Figure 1. a) Schematic fabrication processes of PVA-encapsulation method with four steps: (1) MoS_2 exfoliation on SiO_2 substrate, (2) PVA spin-coating and fully encapsulation of MoS_2 with strong interaction force in between, (3) PVA/MoS_2 released from SiO_2 substrate, (4) bent under strain test equipment with negligible slippage. b) Schematic fabrication processes of the traditional exfoliating method with two steps: (1) MoS_2 direct exfoliation on top of the prefabricated PVA substrate, (2) bent under strain test equipment. a,b) Reproduced under the terms of the CC-BY Creative Commons Attribution 4.0 International license (https://creativecommons.org/licenses/by/4.0).[34] Copyright 2020, The Authors, published by Springer Nature. c) Schematic illustration of the process used to achieve spontaneous and ordered domes. d) Tapping-mode AFM topography of uncoated MoS_2 surface after proton irradiation. e) Tapping-mode AFM topography of patterned HSQ-MoS_2 surface after proton irradiation. c–e) Reproduced with permission.[38] Copyright 2020, Wiley-VCH. f) Formation of random and patterned arrays of MoS_2 domes. Reproduced with permission.[39] Copyright 2020, Wiley-VCH. g) Schematic illustration of AFM tip induced graphene nanobubbles (GNBs). h) Enclosed pattern of GNBs generated through AFM tip using the ramp mode. The tip voltages used to form GNBs located at outer, middle, and inner loops are –8, –7, and –6 V, respectively. i) Bubble display of GNBs formed by AFM tip with voltage ranging from –4 to –9 V working at the contact mode. j) Generation of programmable GNBs with the increase of tip voltage from –4 to –11 V. g–j) Reproduced under the terms of the CC-BY Creative Commons Attribution 4.0 International license (https://creativecommons.org/licenses/by/4.0).[41] Copyright 2019, The Authors, published by Springer Nature.

films. Another advantage of this technique is that the thin film stressors are analogous to SiN_x based stressors, which are implemented in industrial complementary metal-oxide–semiconductor (CMOS) processes to increase Si mobility, implying that this technique is scalable and has the potential to be used for large-scale integration of strain engineered TMDC devices. Interestingly, Di Giorgio et al.[38] exposed mechanically exfoliated MoS_2 flakes on top of a Si/SiO_2 substrate through hydrogen ion irradiation to form hydrogen-filled, micro-and nano-sized spherical membranes (spontaneously

formed domes), which holds a significant, local biaxial strain (Figure 1c–e), reaching up to 7–8%. Similarly, Blundo et al.[39] reported a method to generate a mechanical constraint in MoS_2 monolayers, which led to significant changes in the morphology of the domes (Figure 1f) and enabled periodic giant, nonuniform biaxial strains close to the rupture critical values (>10%). It is worth noting that the highest biaxial strain (12–13%) was achieved in monolayer graphene, which is a benchmark compare to other methods applying strain.[40] However, it should be noted that these high-level strains are not possible for all 2D materials.[33] Among 2D materials, graphene and transition metal dichalcogenides such as MoS_2 stand out to be highly strain tunable so far. Interestingly, Jia et al.[41] developed a method to generate programmable graphene nanobubbles with tunable shape and size at predefined locations using AFM and H atom desorption (Figure 1g–j). This method can be useful to induce predesigned nanobubble with precise size, shape and location as well as to investigate physical phenomena of 2D materials at high magnetic field regimes that do not exist naturally.

2.3. Using Chemical Vapor Deposition Process for Strain Engineering

It is worth noting that conventional strain engineering methods such as heating and mechanical bending cannot conserve strain because of their dependence on external action, which limits the application of 2D materials in strain-electronics. In other words, the generated strain would disappear once the external action is removed, which makes it impossible to further study strain dependent electronic properties. Chen et al.[42] proposed that strain is formed by differences in thermal expansion coefficient between 2D materials and substrates such as between MoS_2 and Si/SiO_2. They developed an optimized method to tune strain during chemical vapor deposition by applying different sulfur removal temperatures. This modified method was experimentally validated to adjust the carrier mobility of monolayer MoS_2 devices as large as two orders of magnitude from ≈ 0.15 to ≈ 23 $cm^2 V^{-1} s^{-1}$. This method should be tested in other 2D materials and heterostructures. It should be noted that Tian et al.[43] reported a different process, that graphene can induce surface reconstruction of Cu which should be generated by partial dislocations in Cu caused by the strain induced by the mechanically very strong graphene overlayer. More research is needed to further explore the varied mechanisms on how the strain is formed between 2D materials and substrates.

3. Tunable Properties of 2D Materials by Strain Engineering

3.1. Tunable Electrical Properties of 2D Materials by Strain Engineering

Effects of strain on electrical transport of 2D materials reveal intriguing physics and future applications.[44–51] Besides several pioneering studies,[46,47] one recent example of such novel physics in strain systems is the work reported by Ho et al.,[49] who demonstrated the introduction of the pseudo-magnetic field in bilayer graphene using a corrugated hBN surface to introduce strain. Low-temperature measurements of the quadratic dependence of second harmonic Hall voltage with current showed clear evidence of Berry curvature change from the strain-induced pseudo-magnetic field. The pseudo-magnetic field also caused a difference in the interlayer and intralayer coupling of the bilayer graphene, resulting in the planar Hall effect (**Figure 2**a). In another example for monolayer graphene,[44] the uniaxial strain of 0.21% induced scalar potential of 0.008 V, causing a shift in the Dirac point. The monolayer graphene was strained using a wedge setup and flexible polyimide substrate (Figure 2b).

Wu et al.[50] used flexible polyimide substrates to strain and demonstrate that odd layer MoS_2 can generate piezo current and voltage when strained at room temperature. The polarity of the induced voltage and current flipped if the direction of strain was rotated by 90°. A strain of 0.53% applied on a single flake resulted in a peak output of 15 mV and 20 pA and an efficiency of 5.08% in conversion of mechanical-to-electrical energy. Polyimide substrates have also been employed to strain transition-metal-dichalcogenide FETs. Shen et al.[45] demonstrated that 1.35% of strain applied on WSe_2 using such a method resulted in a bandgap shift of 100 meV. The bandgap shift was calculated from the change in flat band voltage (Figure 2c,d). Strained $PtSe_2$ using a similar method exhibited more than a 3% resistance change with an applied strain of 0.04%.[51] Using flexible substrate Su-8 instead of polyimide, Park et al. obtained up to 9.78% change in resistance in CVD grown bilayer MoS_2 with a strain of 0.145%. This study investigated the practical application of strain by placing the Su-8 film on the fingertip before introducing strain by bending with pen tips of varying diameters.[52]

2D materials that show phase transition from semiconducting to metallic are potentially applicable in logic transistors, integrated circuits, thermochromic windows, and topological devices. Transition metal dichalcogenides (TMDs) are 2D materials that have multiple structural and electronic phases. Zhao et al.[53] theoretically investigated the effect of strain engineering on the phase transition between 2H- and 1T′-$MoTe_2$ and found that the tensile strain along the armchair direction (+3.08%) or compression along with zigzag orientation (−3.40%) is required for phase transition (Figure 2e–j). Furthermore, a combined effect of strain engineering and charge doping was noted; the injected charge significantly affected the critical strain. The critical strain decreases linearly with the increase of the hole-doping concentration.[53] This study presents a strategy for phase engineering in 2D materials.

3.2. Tunable Superconductivity by Strain Engineering

Strain engineering has also been demonstrated theoretically and experimentally to be able to change the superconducting transition temperature (T_c) or superconducting gap-closing temperature (T_g) of conventional and unconventional superconductors.[54–66] For instance, Tresca et al studied the effect of in-plane strain on electronic, mechanical, and magnetic properties

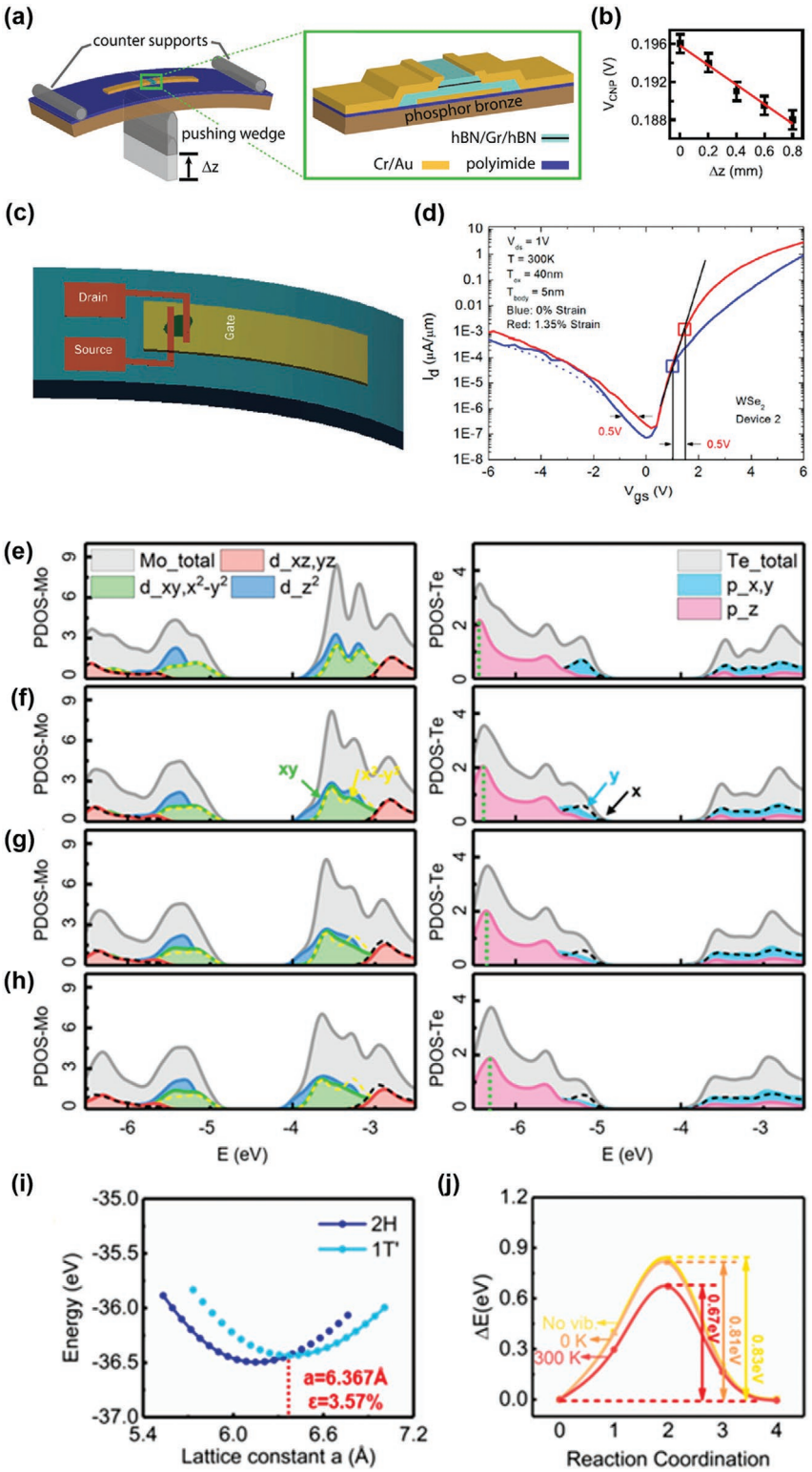

Figure 2. a) Strained graphene on polyimide substrate; b) shift in charge-neutral point due to shifting in Dirac point. a,b) Reproduced under the terms of the CC-BY Creative Commons Attribution 4.0 International license (https://creativecommons.org/licenses/by/4.0).[44] Copyright 2021, The Authors, published by Springer Nature. c) Multilayer WSe_2 strained on bent PET showed d) shift in flat-band voltage. c,d) Reproduced with permission.[45] Copyright 2016, American Chemical Society. e–h) Partial density of state of Mo and Te atoms in pristine $MoTe_2$ (e), and $MoTe_2$ under tensile strain ε_a of 1% (f), 2% (g), and 3.57% (h). The green dashed lines indicate the moving of the p_z orbitals. i) Free energies of 2H- and 1T′-$MoTe_2$ monolayer as a function of constant lattice *a*. j) Relative energy profile of the 2H-1T′ transition as a function of the reaction coordination for $MoTe_2$ with critical compression ε_b. e–j) Reproduced with permission.[53] Copyright 2021, Elsevier.

of monolayer FeSe and FeTe on $SrTiO_3$ substrate, using the first-principles density functional theory.[55] This study predicted that both FeSe and FeTe monolayer are mechanically flexible to hold large strains up to 30% and a superconducting transition is expected if FeTe monolayer can be strained higher than 9%.[55] Ge et al. reported that a small tensile strain increased T_c of 2D electride MgONa to 6.15 K using the similar theory.[56] Moreover, Celebonovic et al. performed the ab initio study about the effects of biaxial strain on two superconducting materials including doped graphene and isostructural MgB_2 monolayer.[57] The results showed that biaxial strain caused phonon to soften, affected the total interaction of electrons and phonons, and led to an increase in T_c in both materials.[57] Experimentally, when tensile strain was applied in single-layer FeSe on Nb-doped $BaTiO_3$, a T_g up to 75 K was obtained, which is a record high pairing temperature for both monolayer-thick films and Fe-based superconductor.[54] Lin et al studied the structural and superconducting properties of $FeSe_{0.3}Te_{0.7}$ thin films at different thickness growing on piezoelectric PMN-PT substrates,[58] where strain can be introduced during growth but also controlled by electric field (post-growth). The results showed that biaxial tensile strain exists in the thin films and the strain relaxed with the increase of film thickness.[58] When the film thickness is larger than 200 nm, the strain was fully relaxed (**Figure 3**a–d).[58] This study also indicated that electric field increased the T_c of the thin film, which is caused by the reduced tensile strain.[58] In a follow up study, Mei et al. developed a two-step growth method to obtain high quality $FeSe_{0.5}Te_{0.5}$ thin films on PMN-PT substrate and this high quality heterostructure enabled to achieve a remarkable tuning in T_c induced by electric field at 20 nm $FeSe_{0.5}Te_{0.5}$ thin film.[59] Strain has also been reported to be able to control superconductivity in few-layer $NbSe_2$ system when grown on insulating substrates (Figure 3e) [60] These studies demonstrated that superconductivity and change in T_c can be realized through strain engineering in 2D superconductors.

While this review mainly focuses on 2D materials, it is of interest to mention that there are also many examples demonstrating that strain could affect the electronic properties of bulk superconductors. Under a uniaxial strain (≈0.6%), T_c of Sr_2RuO_4 enhanced from 1.5 kelvin (K) to 3.4 K.[61] Ivashko et al.[62] have showed that strain engineering can be useful to affect the T_c of Mott-insulating La_2CuO_4. Diamond, which could turn into a superconductor with a $T_c \approx 4$ K, with the increase of compression-shear strain, its T_c was predicted to be able to reach 12.4 K.[63] Also, the T_c of zirconium nitride (ZrN) was predicted to increase from 10.0 to 17.1 K under tensile strains.[64] The potential of strain engineering on enhancing superconductivity and ferroelectric quantum criticality has also been recently revealed through plastic deformation of $SrTiO_3$.[65] These examples again demonstrated that there is a great potential of strain engineering for the manipulation of superconducting transition temperature. Epitaxial strain has been shown to be able to change a normal metal to a superconductor by growing RuO_2 thin films on (110)-oriented TiO_2 substrates.[66] This strategy for regulating superconductivity is rationally designed by comparing the density functional theory calculations and results of angle-resolved photoemission spectroscopy experiments,[66] showing promise to generate novel transition-metal superconductors.

3.3. Tunable Electrochemical Properties of 2D Materials by Strain Engineering

Strain engineering of 2D multilayered heterostructures shows great potential for tuning electrochemical properties (including ionic conduction).[67,68] By interface strain engineering of a 2D multilayered $VOPO_4$–graphene heterostructure, Xiong et al. reported a novel type of zero-strain cathode for reversible intercalation of beyond-Li^+ ions (K^+, Na^+, Zn^{2+}, Al^{3+}) (**Figure 4**).[69] When applying the 2D multilayered heterostructures as cathodes, high-performance K^+-ion batteries with a stable reversible capacity of 160 mA h g^{-1} and a high energy density of ≈570 W h kg^{-1} were obtained (Figure 4).[69] This study demonstrated that straining engineering of 2D materials is useful for high-energy storage applications beyond lithium-ion batteries. Strain engineering has been demonstrated to be useful in promoting the catalytic performance of TMDS and noble metal nanosheets as well. Zhang et al. (2022)[70] recently developed an in situ self-vulcanization method to induce biaxial strain to MoS_2 nanoshells through a form of a single-crystalline Ni_3S_2@MoS_2 core–shell heterostructures with controllable layer numbers (1–5 layers). They found that an electrode with bilayer MoS_2 nanoshells exhibits an outstanding hydrogen evolution reaction (HER) activity.[70] Based on both systematical electrochemical analysis and DFT calculations, it is found that the degree of biaxial strain, MoS_2 layer numbers, and the induced sulfur vacancies contribute to the increased catalytic activity.[70] This study is useful for preparing biaxially strained TMDs electrodes with tunable layer numbers for improving electrocatalytic performance. In a broader context of thin films, we noted that Wu et al. (2022)[71] reported a simple strategy to induce the planar strain in ultrathin noble metal nanosheets by creating amorphous–crystalline phase boundaries which could expose the active strained interfaces. These boundaries induced ≈4% of surface tensile strain in the nanosheets. The strained Ir nanosheets (denoted as AC-Ir NSs) showed about 4.5-fold higher intrinsic HER activity than the benchmark commercial Pt/C catalyst.[71] The underlying mechanism as calculations by density functional theory indicated that the d-band states and hydrogen adsorption performance of the strained Ir nanosheets are optimized by the introduced tensile strain, which thereby enhanced catalysis.[71] Subsequently, this in-plane strain engineering approach has been demonstrated to extendable to other noble metal nanosheets including those of Ru and Rh,[71] suggesting this is a general method with the ability to manipulate the spatial distribution of in-plane strain to improve the hydrogen evolution performance in various ultrathin noble metal nanosheets. It would be interesting to explore and extend such studies in 2D materials, including for other types of catalysis such as oxygen evolution reaction. All these examples revealed the great potential of strain engineering in tuning and improving the electrochemical activities and electrocatalytic performance of 2D materials.

3.4. Tunable Magnetic Properties of 2D Materials by Strain Engineering

In the past several years, besides theoretical and computational studies, a plethora of experimental investigations have

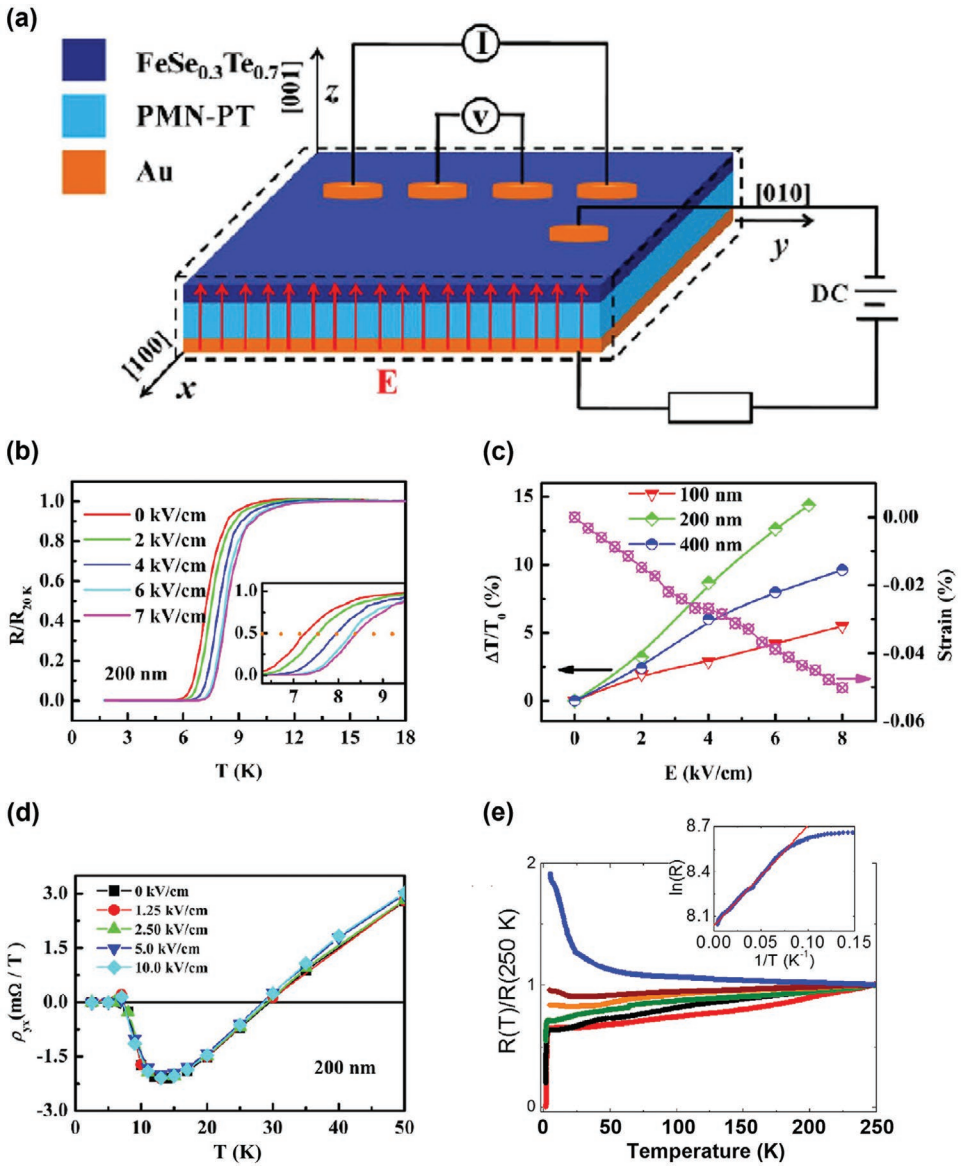

Figure 3. a–d) Control of superconductivity of $FeSe_{0.3}Te_{0.7}$ thin films on PMN-PT by electric-field, which caused reduction in tensile strain and e) strain-modulated superconductivity in few-layer $NbSe_2$. a) Illustration of $FeSe_{0.3}Te_{0.7}$ films grown on PMN-PT substrate. b) Curves of superconducting transition under different electric fields for a 200 nm thick $FeSe_{0.3}Te_{0.7}$ thin films. The inlet figure displays the magnification of image nearby the transition. c) Changes in T_c for $FeSe_{0.3}Te_{0.7}$ films with different strain of PMN-PT with electric field and film thickness. d) Temperature-dependent Hall resistance of $FeSe_{0.3}Te_{0.7}$ film at different electric fields. e) Different growth temperature (from 400 to 600 °C) systematically tuned the $NbSe_2$ samples from the superconductor to insulator transition as shown by resistance measurements. Inset: plot of the ln(R) versus 1/T from the insulating sample. The linear fit works in the full range of temperatures from 13 K and above, giving an excitation gap of $E_0/k_B \approx 6.7$ K. a–d) Reproduced under the terms of the CC-BY Creative Commons Attribution 4.0 International license (https://creativecommons.org/licenses/by/4.0).[58] Copyright 2015, The Authors, published by Springer Nature. e) Reproduced with permission.[60] Copyright 2020, American Chemical Society.

shown that strain engineering is an effective way to tune the magnetic properties of 2D materials.[24,48,72–97] For example, changing the sign of spin–spin exchange interactions in materials with magnetic order can switch between ferromagnetic (FM) and antiferromagnetic (AFM) phases, allowing novel types of magnetoresistive devices. It has been recently reported that atomically thin vdW magnets provide a new system to modify magnetic properties in electrical or nanomechanical ways. Although a switch from AFM to FM states has been reported in the A-type antiferromagnet CrI_3 at zero magnetic fields,[81,88] the phase transition is nonreversible. Moreover, magnetic phase transitions under strain in vdW magnets, though very little experimentally explored, was predicted in multiple studies.[53,84,91,92] Phase transitions have been experimentally demonstrated in thin membranes of 2D antiferromagnetic $FePS_3$, $NiPS_3$ and $MnPS_3$, which can be probed by nanomechanical resonators.[86] This study further revealed that the observed strong relationship between antiferromagnetic order and mechanical motion in ultrathin membranes of 2D materials was mediated by the specific heat, and the Néel

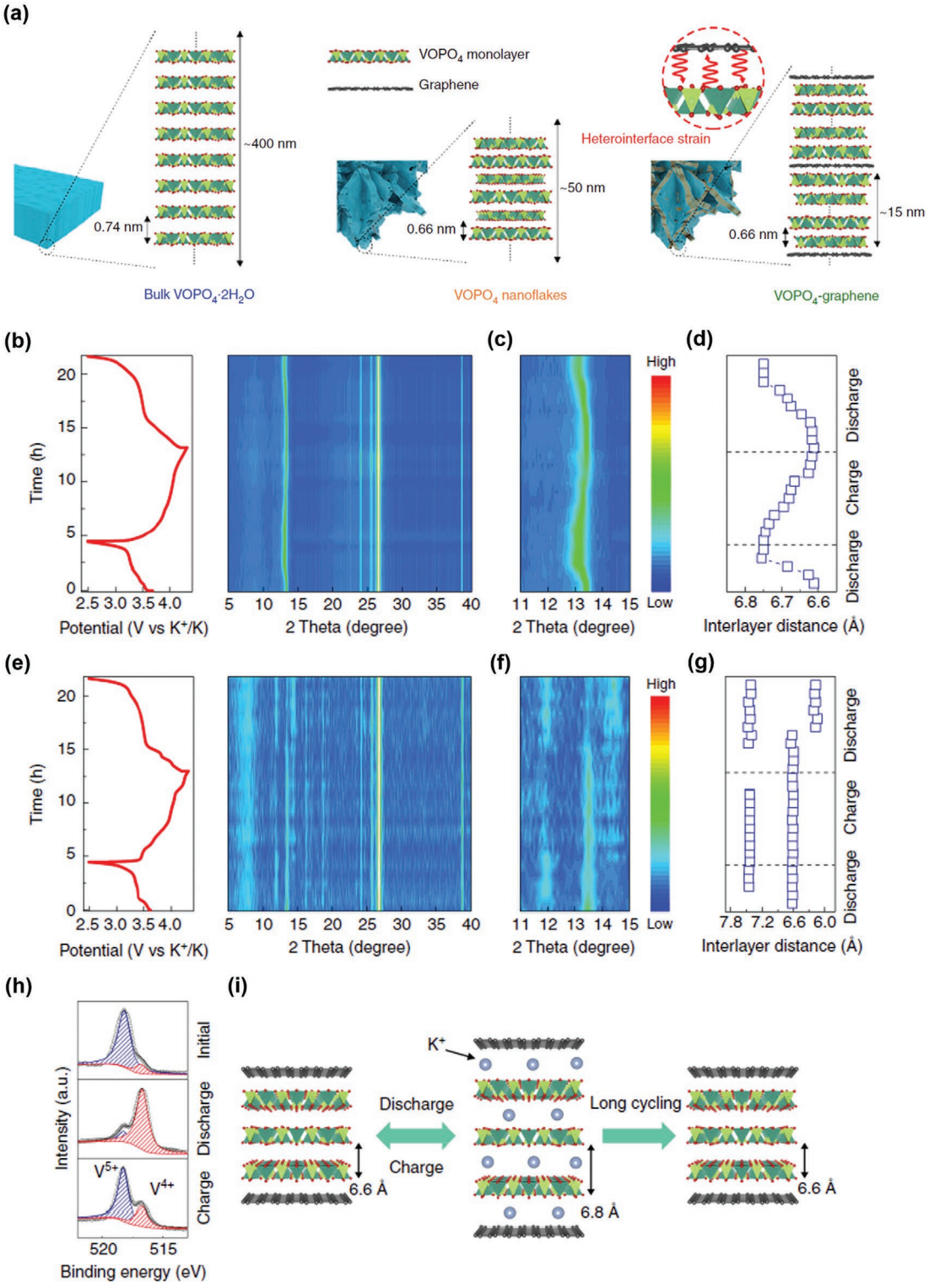

Figure 4. Bulk $VOPO_4{\cdot}2H_2O$, $VOPO_4$ nanoflakes, and $VOPO_4$–graphene, and K^+ ions' zero-strain intercalation. a) Different restacking and interlayer lengths for bulk $VOPO_4{\cdot}2H_2O$, $VOPO_4$ nanoflakes, and $VOPO_4$–graphene. b) Profiles of charge/discharge and in situ X-ray diffraction (XRD) patterns of $VOPO_4$–graphene. c) Enlarged in situ XRD patterns of $VOPO_4$–graphene from 11° to 15°. d) $VOPO_4$–graphene's interlayer distance. e) Profiles of charge/discharge and in situ XRD patterns of $VOPO_4$ nanoflakes as cathodes for potassium-ion batteries. f) Enlarged in situ XRD patterns of $VOPO_4$ nanoflakes. g) $VOPO_4$ nanoflakes' interlayer distance. h) Ex situ V 2p X-ray photoelectron spectroscopy of $VOPO_4$–graphene in different states including initial, discharged, and charged status. i) Proposed mechanism of reversible intercalation of K^+ ions for $VOPO_4$–graphene based 2D multilayered heterostructure. a–i) Reproduced under the terms of the CC-BY Creative Commons Attribution 4.0 International license (https://creativecommons.org/licenses/by/4.0).[69] Copyright 2020, The Authors, published by Springer Nature.

temperature of $FePS_3$ highly depend on electrostatically induced strain (**Figure 5**).[86] This technique is especially useful for the characterization phase transitions of ultrathin membranes and expected to be applicable to 2D ferromagnets, thin 2D complex oxide sheets, organic antiferromagnets and other van der Waals materials.

Interestingly, a reversible strain-induced magnetic phase transition has been recently achieved in a vdW magnet. Cenker et al.[74] reported that the magnetic properties of the A-type layered antiferromagnetic semiconductor CrSBr could be modified by the application of a continuous, in situ uniaxial tensile strain, which reached several percent at cryogenic temperatures. To apply considerable strain on thin vdW flakes, the authors cleaved a silicon substrate to generate a microscopic gap that can suspend a sample. The authors used this newly designed platform to achieve a reversible magnetic phase transition between AFM to FM states induced by strain at zero magnetic fields. Furthermore, this study reported that strain resulted in significant changes in the spin-canting process under an applied out-of-plane magnetic field, demonstrating that strain can control both the saturating field and spin-canting process. These results provide new opportunities to control magnetism and other electronic states in 2D materials and heterostructures by strain engineering, opening potential applications such as strain-actuated magnetoresistive switches, strain tuning of second-harmonic generation through control of magnetic-state-induced inversion symmetry breaking, and strain-controlled magnetic tunnel junctions that operate without an applied magnetic field. The authors think that the strain systems employed in this study should be further applicable in other 2D materials and heterostructures to control their electronic, structural, optical, and magnetic properties, which remain to be fully demonstrated in the future.

In another study, the magnetic properties of vdW ferromagnet $Cr_2Ge_2Te_6$ and its heterostructures $Cr_2Ge_2Te_6$/NiO, including hysteresis loops and Curie temperature (T_C) of $Cr_2Ge_2Te_6$, have been systemically investigated.[80] The results showed that $Cr_2Ge_2Te_6$/NiO exhibited enhanced magnetic perpendicular anisotropy and T_C. The maximum T_C was about 120 K, which is onefold higher than in $Cr_2Ge_2Te_6$ only.[80] Moreover, it was found that the T_C was increased in $Cr_2Ge_2Te_6$/NiO with the $Cr_2Ge_2Te_6$ thickness ranging from 5 to 200 nm.[80] The enhanced magnetic anisotropy and T_C were attributed to strain in $Cr_2Ge_2Te_6$ induced by interfacing with NiO. These results demonstrated that the utilization of heterostructure and interface with other materials helps control the magnetic properties of 2D materials.

Another recent theoretical study by Hu et al.[78] investigated the effect of strain on the magnetic properties of Fe_3GeTe_2 (FGT) monolayers. It demonstrated that ferromagnetism can be enhanced to a large extent by tensile strain in FGT monolayers. In FGT monolayers, ferromagnetism can be improved mainly due to the competing effects of direct exchange and superexchange interactions. The average magnetic moment of the iron atoms increases monotonically with increasing biaxial strain from −5% to 5% in the FGT monolayer (**Figure 6**).

For conventional materials, growing thin films on substrates with various lattice mismatches is a common way to induce lattice strain.[98] For example, perovskite manganites, a class of materials with interesting magnetic properties and colossal magnetoresistance (CMR, where the resistivity decreases significantly in magnetic fields), have received extensive attention in this context due to their potential application in multifunctional devices and the complicated physical mechanism underlying the influence of strain on their electronic and magnetic properties. Heteroepitaxial composites of manganite/ferroelectric (FE) have emerged recently as one platform to study and harness such tunable properties.[99,100] Piezoelectric substrates such as $Pb(Mg_{1/3}Nb_{2/3})$ and O_3-$PbTiO_3$ (PMN-PT) have also been used to introduce strain in heterostructures involving the manganites.[101,102] Also, the ferroelectric ceramic material $BaTiO_3$ superlattices have been shown to induce strain when integrated into silicon and affect the magnetism of $LaMnO_3$ with the change of $BaTiO_3$ thickness.[98] In principle, such piezoelectric substrates should offer a promising method for electrically straining and tuning magnetic properties of 2D magnets, offering a platform to elucidate and explore the rich interplay between electric, magnetic, and lattice degrees of freedom in such artificial "multiferroic" heterostructures.

The Ruddlesden–Popper series of ruthenates $Sr_{n+1}Ru_nO_{3n+1}$, which can be considered a layered material, show excellent magnetic and electronic properties. Their ferromagnetic tendencies are generally strengthened by increasing the number n of RuO_2 sheets per unit cell.[103] The single-layer $n = 1$ compound Sr_2RuO_4 has been extensively investigated for its unconventional superconductivity and magnetism.[104–108] In contrast, the ferromagnetic metal $SrRuO_3$ (SRO) has promising physical properties, including vertical hysteretic shift, magnetocrystalline anisotropy, exchange bias, and anomalous Hall effect for potential utilization in magnetic tunnel junctions and spin valves.[87,102] SRO films' lattice degree of freedom has been considered to offer a significant way to change their physical properties through external fields. For instance, lattice strain-mediated electric-field regulation of magnetic and electrical properties was achieved when an in-plane compressive strain was imposed on SRO films epitaxially grown on PMN-PT single crystals through the piezoelectric response.[109,110]

3.5. Tunable Optical Properties of 2D Materials by Strain Engineering

3.5.1. Strain Tuning of Optical Emission

The first single-photon emitters (SPEs) in 2D materials were discovered 6 years ago.[111–113] Local strain has been applied to induce such quantum emitters in TMDC and hexagonal boron nitride (h-BN).[114] For example, So et al.[115] have used local strain to induce electrically driven deterministic SPEs in a vdW heterostructure including graphene, h-BN, and WSe_2. Parto et al.[116] reported a method to create site-controlled SPEs in atomically thin WSe_2 using simultaneous and independent strain engineering with nanoscale stressors and defect engineering through electron-beam irradiation. Emitters showed biexciton cascaded emission, and the highest purity of single-photon reached over 95%, and the highest working temperature reached up to 150 K (**Figure 7**).[116]

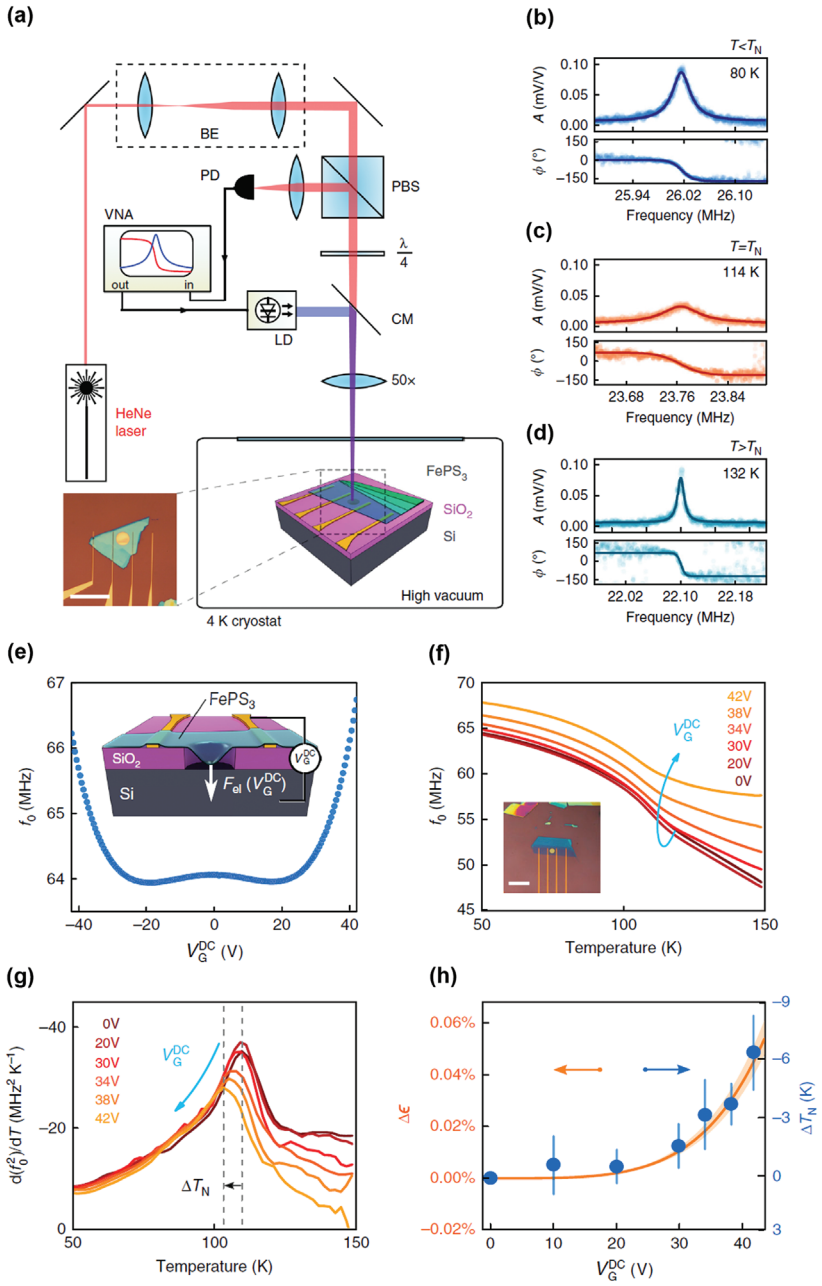

Figure 5. Mechanical resonances of a thin antiferromagnetic $FePS_3$ membrane and gate voltage tuned resonance frequency and transition temperature. a) Setup of laser interferometry. Blue actuation laser diode λ_{blue} is 405 nm, red interferometric detection laser λ_{red} is 632 nm. CM, cold mirror; LD, laser diode; PBS, polarizing beam splitter; PD, photodiode; VNA, vector network analyzer. Inset: optical picture of $FePS_3$ membrane including electrodes for electrostatic control of strain. Membrane diameter d is 10 µm; flake thickness is 45.2 ± 0.6 nm. b–d) Phase (ϕ) and amplitude (A) of the fundamental resonance for the device at three various temperatures. Solid lines, fit of the mechanical resonance utilized to obtain f_0 and Q; filled dots, measured results. e) Resonance frequency is shown as a function of gate voltage at 50 K. Inset: illustration of the electrostatic tuning. f) Resonance frequency at six voltages, as a function of temperature; Inset: optical picture of the device, t is 8 ± 0.5 nm. Scale bar: 16 µm. g) Derivative of f_0^2 as a function of temperature and gate voltage. h) The blue solid dots shows changes in T_N as a role of V_G^{DC} obtained from the peak position in (f). The orange solid line shows the pattern of electrostatically induced strain as a function of V_G^{DC}. a–h) Reproduced under the terms of the CC-BY Creative Commons Attribution 4.0 International license (https://creativecommons.org/licenses/by/4.0).[86] Copyright 2020, The Authors, published by Springer Nature.

Furthermore, Mukherjee et al.[117] reported the observation of electric field tuned SPEs at positions where strain is induced using WSe_2, hBN, and few-layer graphene on a nanopillar array. They found that the emission energies were increased (blueshift) in those strain-induced emitters, in contrast to previous studies, which showed reduction in energy of randomly occurring quantum emitters in WSe_2.[117] It is noted that the trap potential of volume and depth still vary broadly among the various nanopillar sites on the same array. Hence, further experiments are needed to explore the exact physical origin of the

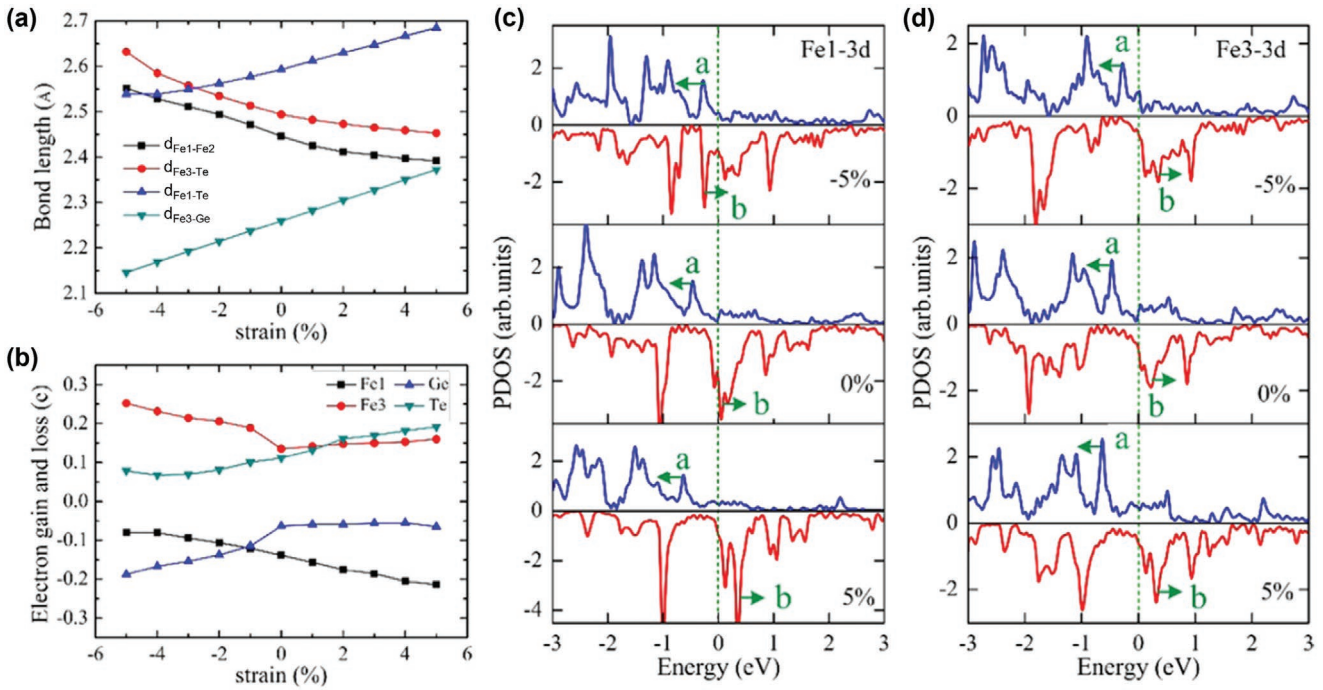

Figure 6. a) Strain dependence of the distance and the bonding length (Fe1–—Fe2 distance, $d_{Fe1-Fe2}$; Fe3—Te bond length, d_{Fe3-Te}; Fe1–Te bond length, d_{Fe1-Te}; Fe3–Ge bond length, d_{Fe3-Ge}). b) Electron transfer of Fe, Ge, and Te atoms in the FGT monolayer. c,d) PDOS of Fe1 atom (c) and Fe3 atom (d) in the FGT monolayer under −5%, 0%, and 5% biaxial strain, respectively. The blue and red solid lines indicate spin-up and spin-down channels, respectively. a–d) Reproduced with permission.[78] Copyright 2020, American Chemical Society.

sign and magnitude of the volume of different traps. In another study, Xu et al.[118] reported radiation- and lithography-free method to deterministically activate hBN SPEs using atomic force microscopy nanoindentation; the maximum yield of SPEs reached 36% for an indent size of 400 nm. This method used hBN flakes on flat silicon dioxide–silicon substrates (Si/SiO_2), which has the potential to be easily applied to on-chip photonic devices.[118] While the exact nature of such indentation-induced SPEs remain to be better understood, the author suggested that the creation of structural edges and highly strained hBN local areas near the indents may both play roles for the high SPE yield achieved.[118] These studies present new ways to generate deterministic SPEs, which are helpful for the practical application of integrated quantum light sources. Also, biaxial strain has been applied through strain transfer from a PMN-PT substrate to quantum emitters consisting of few-layer graphene, h-BN, and a monolayer WSe_2 flake.[119] With the change of biaxial strain on these emitters, the authors noted that the emission axis rotated by about 40°, and a maximum energy change up to 10 meV.[119]

Significant progress has been made in this area, and SPE metrics, including purity, brightness, and indistinguishability, have increased during the past several years. On the other hand, future directions should include a better understanding of the trap volumes, depths, widths, and stabilities of SPEs, as well as more detailed mechanisms on how optical properties of 2D materials could be regulated by strain or defect engineering to achieve reversible, positional-deterministic and stable SPEs for their application for solid-state quantum light sources.

3.5.2. Strain Tuning of Photoconduction and Photocurrent

Recent work showed that 2D indium chalcogenides such as α-In_2Se_3 and InS_2 are great candidates for next-generation optoelectronic-related devices. Still, traditional 2D indium chalcogenide devices on SiO_2 substrates' performance are limited by the substrate's detrimental effect, which significantly restricts charge transport. While an internal electric field could alleviate the situation, interface defects are inevitably introduced using conventional stacking technology. Yang et al.[120] developed a universal and simple structure for generating highly sensitive photodetectors and optimized this structure through a combination of strain and interface engineering. A SiO_2 window was generated to afford a "suspended" α-In_2Se_3 channel, which effectively decreased the detrimental effects of the substrate. Moreover, this method induced local strain in the suspended α-In_2Se_3, regulating the band structure and causing an intramolecular type-II alignment.[120] Subsequently, the interfacial charge transfer was optimized, and the photodetection performance was improved. The device showed excellent photosensitivity with a responsivity of 1672 A W^{-1}, an on/off ratio of 263, a detectivity of 7.5×10^{13} Jones, and a relatively quick response rate with 12 ms for both decay and rise.[120] The broad application potential of the proposed approach has been tested, and results showed that this method could be extended to InSe devices to improve their photodetection capability. This study provides another strategy to improve the development of high-performance photodetectors based on 2D materials; whether it applies to other 2D material-based photodetectors beyond the ones studied is to be determined. In addition,

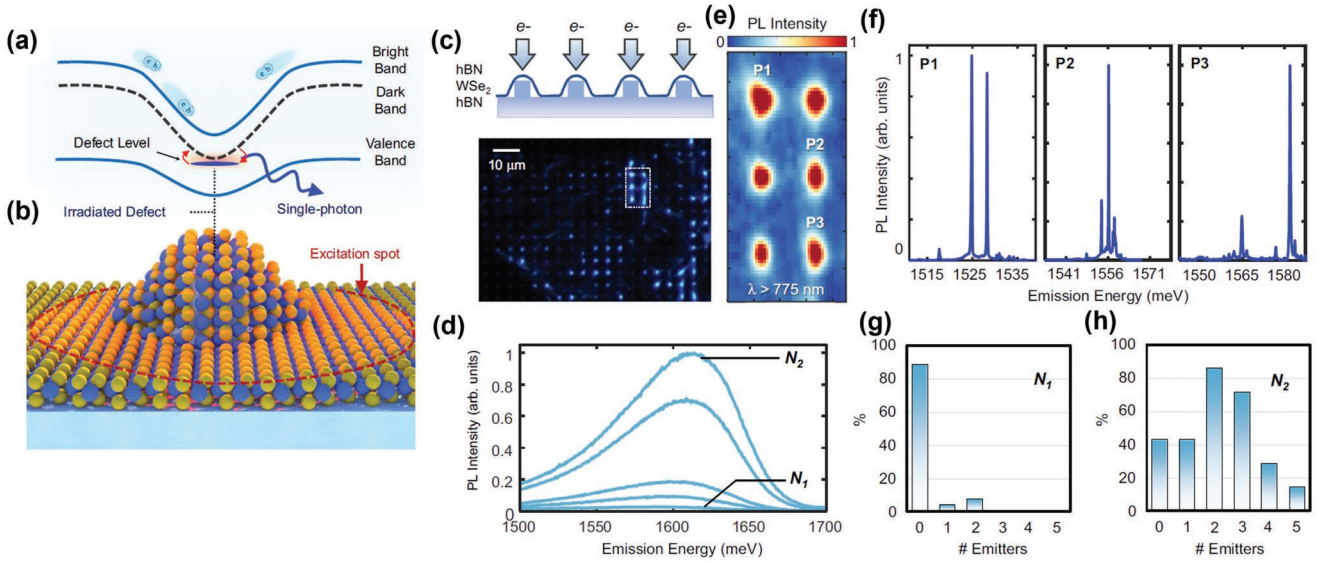

Figure 7. a,b) Defect and strain-engineered WSe_2 single-photon emitters (SPE). c–h) Site-controlled quantum emitter array through the defect and strain engineering, i–k) electrically driven SPE formed by AFM indentation, and l–n) splitting of fine structure from the single-photon emission. a) Changes in the spatial bandgap caused by strain (dashed gray line means the dark excitonic band; the solid blue lines represent valence band and bright band, respectively). b) Overview of 1L-WSe_2 strained on a SiO_2 nanopillar (seen in yellow and W atoms displayed in blue). Neutral excitons shown as e–h pairs, generated within the excitation laser spot, indicated by th red dashed line, funnel to strain regions with low potential. There is also a dark-exciton band from WSe_2 at energies lower than the bright exciton, which is optically prohibited by the transition selection of WSe_2. The dark-exciton can be strain-tuned to a defect-level becoming intervalley defect excitons when there is a defect (on the top of irradiated nanopillar represented by a blue dash) and at strained regions. c) Overview of the prepared structure and the sample's optical dark-field image. A stack of h-BN/WSe_2/h-BN was transferred to the SiO_2 nanopillar array. Because of exciton funneling, bright emission was noted from the pillar top. Then, the top of pillars was irradiated (arrows indicating e^- arrows) to generate structural defects. d) PL spectra showing unstrained WSe_2 defect-bound excitons for different irradiation intensity ranging from $N_1 = 10^5$ electrons μm^{-1} to $N_2 = 10^6$ electrons μm^{-1}. e) PL map of irradiated and strained sites integrated spectrally for wavelengths over 775 nm, indicating the bright emission related to SPEs. Some places held more than one emitter and reached saturation incident count. Because of the localized nature of the emitters, the maps are similar to the Gaussian spots of excitation laser; f) PL spectrum (1 μW excitation power) taken from various sites indicating the sharp emission lines (75 μeV average linewidths) related to SPEs. Note: many strong emission lines are present in pairs, suggesting that exciton–biexciton pairs formed. g,h) Histograms of the number of quantum emitters tested per site through irradiating with e-beam intensity of 10^5 and 10^6 electrons μm^{-2}, respectively. i) Overview of the vertical heterostructure including top graphene/WSe_2/h-BN/bottom graphene on the polymer substrate, with the emission site indented by an AFM tip. j) Overview of the strained heterostructure bands after applied external bias. E_B, E_D, E_V, and E_{Defect} are excitonic bright band, dark excitonic band, valence band, and defect state of WSe_2, respectively. On the right panel, the dashed red and solid lines represent the changes in spatial bandgap resulting from strain. The strain-localized dark exciton was mixed with a defect state, leading to the generation of a localized defect exciton; k) fabrication process; l) electroluminescence (EL) spectrum with high resolution measured at a selected indentation site. A separation of ≈400 μeV and a linewidth of 755 μeV exists in observed fine structure splitting. m) Normalized EL intensities of the higher (red) and lower (black) energy peaks that indicated by corresponding color arrows in (l), as a role of the angle of polarization. The fitted curves are shown by the lines. The polarization degrees and angles are 0.965° and 148° (red) and 0.946° and 56° (black), respectively; n) EL spectrum of (l) as a role of angle of polarization. a–h) Reproduced under the terms of the CC-BY Creative Commons Attribution 4.0 International license (https://creativecommons.org/licenses/by/4.0).[116] Copyright 2021, The Authors, published by Springer Nature.

strain engineering has been reported to regulate photoresponse of a 2D α-In_2Se_3/WSe_2 vdW heterostructure and 2D hybrid perovskite ferroelectric single-crystalline thin-films.[121,122] For instance, with the introduction of 0.433% of tensile strain, the photocurrent of the photodetector (α-In_2Se_3/WSe_2 vdW heterostructure) increased around 18-folds. Moreover, excellent photodetectivity and responsivity was achieved in the photodetectors.[121] Because of the noncentrosymmetric structure of III–VI compound α-In_2Se_3, the strain-caused piezopotential affects the band slope close to the P-N junction interface, which thereby enhanced the separation efficiency and transfer characteristics of photogenerated electron–hole pairs through piezophototronic effect.[121] These results suggest the potential of artificial heterostructures and straining in controlling optical properties.

Strain-induced electric fields have been shown to enhance the performance of phototransistor in thin HfS_2 device.[123] The strain was introduced by the formation of HfO_2 using focused laser spots on the device. The induced strain was compressive at HfO_2/HfS_2 interface and tensile away from the interface. In the indirect 2D semiconductor HfS_2, the tensile strain caused charge to funnel away from the oxidized spots. Photoresponsivity of the device was enhanced up to 350% at low power by such a strain profile (**Figure 8**). This study suggests a potential approach to design low-power consumption multifunctional electronic and optical devices based on strain engineering.

The co-effects of the light and electric field on lattice distortion and physical properties of SRO/PMN-PT epitaxial heterostructures were recently tested.[124] Results showed a strong correlation between the electric field and light, as indicated by the tunable resistance and photoresistance effects by light illumination and the electric field, respectively, which was mediated

by strain-driven lattice-orbital coupling.[124] This study suggests a potential approach to design low-power consumption multifunctional electronic and optical devices based on complex oxide heterostructures through strain engineering that may be applicable to various oxide or nonoxide 2D materials.

Du et al.[3] summarized recent progress of strain engineering on the flexible optoelectronics of 2D materials, they commented that a universal method to evaluate flexible optoelectronics of 2D materials among various devices is missing. Finally, six parameters including response time, cutoff wavelength, linear dynamic range, specific detectivity, photoresponsivity, and external quantum efficiency for easy comparison of the performance amongst different devices for further development and success of this area were summarized.

3.5.3. Tuning of Photovoltaics

Strain engineering has also been shown to be an effective strategy to enhance photovoltaics in 2D materials as well as other materials such as halide perovskites theoretically and experimentally.[125–132] Bastonero et al. (2022)[126] proposed a new single-layer heterostructure PdS_2/PtS_2 based on ab initio many-body perturbation theory. It is calculated that this heterostructure shows excellent light absorbance, yielding up to 50% in the visible spectrum and reaching a short-circuit current of 7.2 mA cm^{-2} after solar irradiation.[126] Also, based on first-principles calculations, a 2D α-As/α-AsP vdW heterostructure was shown to be useful for photovoltaic applications under an in-plane strain ranging from –6% to 6%[130] and the photocurrent of the designed bifunctional GeC/SnSSe heterostructure based on first-principles and quantum transport calculations increased by 40% under a 4% tensile strain.[132] Experimentally, the flexo-photovoltaic effect (bulk photovoltaic effect induced by a strain gradient) was demonstrated in an archetypal 2D material, MoS_2, through a strain-gradient engineering method based on structural inhomogeneity and phase transition of MoS_2/VO_2.[133] The bulk photovoltaic coefficient in MoS_2 was found to be orders of magnitude larger than most non-centrosymmetric materials.[133] The relationship between a strain gradient and the flexo-photovoltaic effect in low-dimensional materials shows great potential to explore novel optoelectronic phenomena in strain-gradient-engineered materials for their application in photovoltaics. In another study, with 0.433% strain at 782 μW cm^{-2} intensity of illumination, the photocurrent of the prepared 2D α-In_2Se_3/WSe_2 achieved up to –164 nA, which is 304-folds higher than the I_{dark} examined under nonstrain condition.[121] These studies suggest the great potential of strain engineering in improving photovoltaics toward better photoresponse of devices.

4. Conclusion and Perspectives

We have reviewed the recent progress in the strain engineering of 2D materials including several newly developed methods

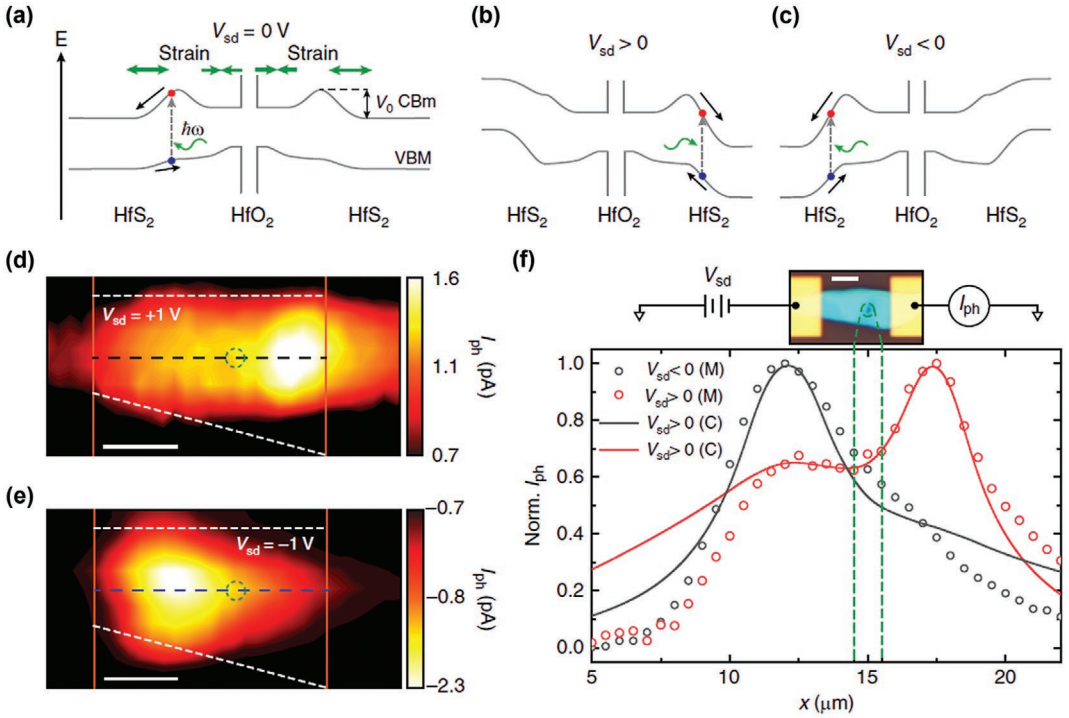

Figure 8. Strain-induced charge funnel effect in HfS_2/HfO_2 device. a) Schematic band illustration of a device under strain induced by local oxidation, with V_{sd} = 0 V. b,c) Schematic band diagrams of the device when $V_{sd}>0$ and $V_{sd}<0$, respectively. d,e) Scanning photocurrent microscopy (SPCM) map of the device when V_{sd} = +1 V and V_{sd} = –1 V, respectively. f) Normalized photoresponse along the channel center in the SPCM maps in panels (d), (e) (dots) as well as simulated curves (solid lines). a–f) Reproduced under the terms of the CC-BY Creative Commons Attribution 4.0 International license (https://creativecommons.org/licenses/by/4.0).[123] Copyright 2018, The Authors, published by Springer Nature.

for inducing strain and highlighting the ability of strain engineering to change the electrical, magnetic, and optical properties of 2D materials. Although the potential application of straining engineering on 2D materials in optical, electronic, and spintronic devices is promising, much more research is still needed in several aspects to further improve their electrical, magnetic, optical properties and their strain tuning. First, methods to induce strain should be further developed and optimized for generating position predictable, constant, repeatable, more significant, and periodic strains. Second, heterostructures show promising and attractive electrical, magnetic, and optical properties. Strain transfer between different layers of heterostructures should be explored with greater scrutiny. To add to that, the interaction and quality of interface between 2D materials and their substrates should be studied more, and the condition for the integration between them should be investigated to a greater degree for better tunable properties. Third, whether some newly developed methods for introducing strain and changing electrical, magnetic, and optical properties demonstrated in a small number of 2D materials are also applicable in other 2D materials remain to be tested. Given that different properties that each 2D material may possess, the methods may need to be adjusted accordingly. Fourth, piezoelectric substrates should provide a promising approach for electrically straining and tuning a variety of 2D materials. One example is using then to turn the magnetic properties of 2D magnets, offering a platform to elucidate and explore the rich interplay between electric, magnetic, and lattice degrees of freedom in such artificial "multiferroic" heterostructures. Fifth, it is worth noting that superconducting and magnetic 2D materials are still underexplored in strain tuning, but motivated by previous studies on strain or pressure effects on superconductors and magnetic materials in general, there should be many opportunities to study the effects of strain on them. Six, regarding the application of strain engineering to optical properties of 2D materials, a better understanding is needed of the trap volumes, depths, widths, and stabilities of SPEs, as well as more detailed mechanisms on how optical properties of 2D materials could be controlled by strain or defect engineering, to achieve reversible, positional-controllable, and stable SPEs for their application for solid-state quantum light sources.

In addition, more work is needed in theoretical research for modeling and predicting the effect and conditions of strain engineering on electrical, magnetic, and optical properties on 2D materials, and a stronger coupling between theory and experimental efforts to better understand the microscopic physical mechanisms at material and device levels and to validate the proposed theoretical model experimentally whenever feasible. Generally, the underlying mechanisms for strain engineering of 2D materials on the influence of device performance of course depend on what specific types of devices.[33,134] For example, for electronic devices such as transistors, the mechanisms for straining tuning of device performance such as transconductance (gate-tunability, on/off ratio) are based on strain tuning of band structure (such as bandgap) and other microscopic electronic transport characteristic (such as carrier mobility). For spintronic devices (involving 2D magnets), strain tuning of device performance can occur via strain tuning of magnetic exchange and anisotropy energies which in turn affects critical field and temperatures for magnetic switching and phase transitions. For photonic devices involving excitons and quantum emitters, the strain tuning can occur due to strain effects to localize excitons and enhance optical transition strength as well as modulating optical band gap (transition energy), etc. Moreover, the emerging AI techniques could be introduced and combined with the theoretical and computational research to generate more universal, effective, and accurate model to with predicting power to better understand and control electrical, magnetic, and optical properties of 2D materials through strain engineering and guide the choice and design of materials and device structures and experimental tests. With a better understanding of all the directions mentioned above, it is expected that the application of straining engineering in optical, electronic, and spintronic devices will be advanced further in the near future.

Acknowledgements

The authors acknowledge partial support of this work by Macau Science and Technology Development Fund (FDCT Grants 0106/2020/A3 and 0031/2021/ITP), Macau University of Science and Technology (FRG-21-034-MISE), and the National Science Foundation (1711332).

Conflict of Interest

The authors declare no conflict of interest.

Author Contributions

Y.Q. and M.A.S. contributed equally to this work. Y.Q. and Y.P.C. contributed to the conceptualization, funding acquisition, supervision, writing the original draft, and writing, reviewing, and editing of the manuscript. M.A.S. contributed to writing the original draft and writing, reviewing, and editing of the manuscript. D.H., Y.J., M.Z., and Z.W. contributed to writing, reviewing, and editing of the manuscript.

Keywords

2D materials, electrochemical properties, magnetic properties, strain engineering, superconducting properties

Received: June 22, 2022
Revised: August 1, 2022
Published online:

[1] Z. Dai, L. Liu, Z. Zhang, *Adv. Mater.* **2019**, *31*, 1805417.
[2] S. Deng, A. V. Sumant, V. Berry, *Nano Today* **2018**, *22*, 14.
[3] J. Du, H. Yu, B. Liu, M. Hong, Q. Liao, Z. Zhang, Y. Zhang, *Small Methods* **2021**, *5*, 2000919.
[4] A. K. Geim, *Science* **2009**, *324*, 1530.
[5] A. K. Geim, K. S. Novoselov, *Nanosci. Technol.* **2010**, *30*, 11.
[6] A. H. Castro Neto, F. Guinea, N. M. R. Peres, K. S. Novoselov, A. K. Geim, *Rev. Mod. Phys.* **2009**, *81*, 109.
[7] X. Huang, Z. Yin, S. Wu, X. Qi, Q. He, Q. Zhang, Q. Yan, F. Boey, H. Zhang, *Small* **2011**, *7*, 1876.
[8] R. Mas-Balleste, C. Gomez-Navarro, J. Gomez-Herrero, F. Zamora, *Nanoscale* **2011**, *3*, 20.

[9] A. Gupta, T. Sakthivel, S. Seal, *Prog. Mater. Sci.* **2015**, *73*, 44.
[10] M. Gibertini, M. Koperski, A. F. Morpurgo, K. S. Novoselov, *Nat. Nanotechnol.* **2019**, *14*, 408.
[11] K. S. Novoselov, A. Mishchenko, A. Carvalho, A. H. Castro Neto, *Science* **2016**, *353*, 461.
[12] A. Chaves, J. G. Azadani, H. Alsalman, D. R. Da Costa, R. Frisenda, A. J. Chaves, S. H. Song, Y. D. Kim, D. He, J. Zhou, A. Castellanos-Gomez, F. M. Peeters, Z. Liu, C. L. Hinkle, S.-H. Oh, P. D. Ye, S. J. Koester, Y. H. Lee, Ph. Avouris, X. Wang, T. Low, *npj 2D Mater. Appl.* **2020**, *4*, 29.
[13] B. L. Chittari, D. Lee, N. Banerjee, A. H. Macdonald, E. Hwang, J. Jung, *Phys. Rev. B* **2020**, *101*, 085415.
[14] Z. Dai, N. Lu, K. M. Liechti, R. Huang, *Curr. Opin. Solid State Mater. Sci.* **2020**, *24*, 100837.
[15] C. Di Giorgio, E. Blundo, G. Pettinari, M. Felici, F. Bobba, A. Polimeni, *Adv. Mater. Interfaces* **2022**, *9*, 2102220.
[16] Y. Guo, B. Wang, X. Zhang, S. Yuan, L. Ma, J. Wang, *InfoMat* **2020**, *2*, 639.
[17] W. He, L. Kong, W. Zhao, P. Yu, *Coatings* **2022**, *12*, 122.
[18] P. Huang, P. Zhang, S. Xu, H. Wang, X. Zhang, H. Zhang, *Nanoscale* **2020**, *12*, 2309.
[19] Y. Khan, Sk. Md. Obaidulla, M. R. Habib, A. Gayen, T. Liang, X. Wang, M. Xu, *Nano Today* **2020**, *34*, 100902.
[20] T. Lan, B. Ding, B. Liu, *Nano Sel.* **2020**, *1*, 298.
[21] Z. Qian, L. Jiao, L. Xie, *Chin. J. Chem* **2020**, *38*, 753.
[22] S. I. Vishkayi, Z. Torbatian, A. Qaiumzadeh, R. Asgari, *Phys. Rev. Mater.* **2020**, *4*, 094004.
[23] M.-C. Wang, C.-C. Huang, C.-H. Cheung, C.-Y. Chen, S. G. Tan, T.-W. Huang, Y. Zhao, Y. Zhao, G. Wu, Y.-P. Feng, H.-C. Wu, C.-R. Chang, *Ann. Phys.* **2020**, *532*, 1900452.
[24] Z. Wu, J. Hao, *npj 2D Mater. Appl.* **2020**, *4*, 4.
[25] X. Wu, X. Chen, R. Yang, J. Zhan, Y. Ren, K. Li, *Small* **2022**, *18*, 2105877.
[26] S. Yang, Y. Chen, C. Jiang, *InfoMat* **2021**, *3*, 397.
[27] W. Yu, K. Gong, Y. Li, B. Ding, L. Li, Y. Xu, R. Wang, L. Li, G. Zhang, S. Lin, *Small* **2022**, *18*, 2105383.
[28] S. Zhang, R. Xu, N. Luo, X. Zou, *Nanoscale* **2021**, *13*, 1398.
[29] F. Guinea, *Solid State Commun.* **2012**, *152*, 1437.
[30] M. A. Bissett, M. Tsuji, H. Ago, *Phys. Chem. Chem. Phys.* **2014**, *16*, 11124.
[31] R. Roldán, A. Castellanos-Gomez, E. Cappelluti, F. Guinea, *J. Phys.: Condens. Matter* **2015**, *27*, 313201.
[32] C. Si, Z. Sun, F. Liu, *Nanoscale* **2016**, *8*, 3207.
[33] E. Blundo, E. Cappelluti, M. Felici, G. Pettinari, A. Polimeni, *Appl. Phys. Rev.* **2021**, *8*, 021318.
[34] Z. Li, Y. Lv, L. Ren, J. Li, L. Kong, Y. Zeng, Q. Tao, R. Wu, H. Ma, B. Zhao, D. Wang, W. Dang, K. Chen, L. Liao, X. Duan, X. Duan, Y. Liu, *Nat. Commun.* **2020**, *11*, 1151.
[35] S. Mikael, J.-H. Seo, D.-W. Park, M. Kim, H. Mi, A. Javadi, S. Gong, Z. Ma, *Extreme Mech. Lett.* **2017**, *11*, 77.
[36] F. Colangelo, A. Pitanti, V. Mišeikis, C. Coletti, P. Pingue, D. Pisignano, F. Beltram, A. Tredicucci, S. Roddaro, *2D Mater.* **2018**, *5*, 045032.
[37] T. Peña, S. A. Chowdhury, A. Azizimanesh, A. Sewaket, H. Askari, S. M. Wu, *2D Mater.* **2021**, *8*, 045001.
[38] C. Di Giorgio, E. Blundo, G. Pettinari, M. Felici, Y. Lu, A. M. Cucolo, A. Polimeni, F. Bobba, *Adv. Mater. Interfaces* **2020**, *7*, 2001024.
[39] E. Blundo, C. Di Giorgio, G. Pettinari, T. Yildirim, M. Felici, Y. Lu, F. Bobba, A. Polimeni, *Adv. Mater. Interfaces* **2020**, *7*, 2000621.
[40] C. Lee, X. Wei, J. W. Kysar, J. Hone, *Science* **2008**, *321*, 385.
[41] P. Jia, W. Chen, J. Qiao, M. Zhang, X. Zheng, Z. Xue, R. Liang, C. Tian, L. He, Z. Di, X. Wang, *Nat. Commun.* **2019**, *10*, 3127.
[42] Y. Chen, W. Deng, X. Chen, Y. Wu, J. Shi, J. Zheng, F. Chu, B. Liu, B. An, C. You, L. Jiao, X. Liu, Y. Zhang, *Nano Res.* **2021**, *14*, 2314.
[43] J. Tian, H. Cao, W. Wu, Q. Yu, N. P. Guisinger, Y. P. Chen, *Nano Lett.* **2012**, *12*, 3893.
[44] L. Wang, A. Baumgartner, P. Makk, S. Zihlmann, B. S. Varghese, D. I. Indolese, K. Watanabe, T. Taniguchi, C. Schönenberger, *Commun. Phys.* **2021**, *4*, 147.
[45] T. Shen, A. V. Penumatcha, J. Appenzeller, *ACS Nano* **2016**, *10*, 4712.
[46] N. Levy, S. A. Burke, K. L. Meaker, M. Panlasigui, A. Zettl, F. Guinea, A. H. C. Neto, M. F. Crommie, *Science* **2010**, *329*, 544.
[47] F. Guinea, M. I. Katsnelson, A. K. Geim, *Nat. Phys.* **2010**, *6*, 30.
[48] A. Bafekry, C. Stampfl, S. Farjami Shayesteh, *ChemPhysChem* **2020**, *21*, 164.
[49] S.-C. Ho, C.-H. Chang, Y.-C. Hsieh, S.-T. Lo, B. Huang, T.-H.-Y. Vu, C. Ortix, T.-M. Chen, *Nat. Electron.* **2021**, *4*, 116.
[50] W. Wu, L. Wang, Y. Li, F. Zhang, L. Lin, S. Niu, D. Chenet, X. Zhang, Y. Hao, T. F. Heinz, J. Hone, Z. L. Wang, *Nature* **2014**, *514*, 470.
[51] S. Wagner, C. Yim, N. Mcevoy, S. Kataria, V. Yokaribas, A. Kuc, S. Pindl, C.-P. Fritzen, T. Heine, G. S. Duesberg, M. C. Lemme, *Nano Lett.* **2018**, *18*, 3738.
[52] M. Park, Y. J. Park, X. Chen, Y.-K. Park, M.-S. Kim, J.-H. Ahn, *Adv. Mater.* **2016**, *28*, 2556.
[53] Y. Zhao, Y. Li, S. He, F. Ma, *Chem. Phys. Lett.* **2021**, *770*, 138473.
[54] R. Peng, H. C. Xu, S. Y. Tan, H. Y. Cao, M. Xia, X. P. Shen, Z. C. Huang, C. H. P. Wen, Q. Song, T. Zhang, B. P. Xie, X. G. Gong, D. L. Feng, *Nat. Commun.* **2014**, *5*, 5044.
[55] C. Tresca, F. Ricci, G. Profeta, *2D Mater.* **2014**, *2*, 015001.
[56] Y. Ge, S. Guan, Y. Liu, *New J. Phys.* **2017**, *19*, 123020.
[57] V. Celebonovic, J. Pesic, R. Gajic, B. Vasic, A. Matkovic, *J. Appl. Phys.* **2019**, *125*, 154301.
[58] Z. Lin, C. Mei, L. Wei, Z. Sun, S. Wu, H. Huang, S. Zhang, C. Liu, Y. Feng, H. Tian, H. Yang, J. Li, Y. Wang, G. Zhang, Y. Lu, Y. Zhao, *Sci. Rep.* **2015**, *5*, 14133.
[59] C. Mei, Z. Lin, R. Zhang, C. Xu, H. Huang, Y. Dong, M. Meng, Y. Gao, X. Zhang, Q. Zhang, L. Gu, H. Yang, H. Tian, J. Li, Y. Lu, G. Zhang, Y. Zhao, *ACS Appl. Mater. Interfaces* **2020**, *12*, 12238.
[60] C. Chen, P. Das, E. Aytan, W. Zhou, J. Horowitz, B. Satpati, A. A. Balandin, R. K. Lake, P. Wei, *ACS Appl. Mater. Interfaces* **2020**, *12*, 38744.
[61] A. Steppke, L. Zhao, M. E. Barber, T. Scaffidi, F. Jerzembeck, H. Rosner, A. S. Gibbs, Y. Maeno, S. H. Simon, A. P. Mackenzie, C. W. Hicks, *Science* **2017**, *355*,148.
[62] O. Ivashko, M. Horio, W. Wan, N. B. Christensen, D. E. Mcnally, E. Paris, Y. Tseng, N. E. Shaik, H. M. RÃ¸Nnow, H. I. Wei, C. Adamo, C. Lichtensteiger, M. Gibert, M. R. Beasley, K. M. Shen, J. M. Tomczak, T. Schmitt, J. Chang, *Nat. Commun.* **2019**, *10*, 786.
[63] C. Liu, X. Song, Q. Li, Y. Ma, C. Chen, *Phys. Rev. Lett.* **2020**, *124*, 147001.
[64] W. Lu, H. Zhai, Q. Li, C. Chen, *J. Phys. Chem. Lett.* **2021**, *12*, 1985.
[65] S. Hameed, D. Pelc, Z. W. Anderson, A. Klein, R. J. Spieker, L. Yue, B. Das, J. Ramberger, M. Lukas, Y. Liu, M. J. Krogstad, R. Osborn, Y. Li, C. Leighton, R. M. Fernandes, M. Greven, *Nat. Mater.* **2022**, *21*, 54.
[66] J. P. Ruf, H. Paik, N. J. Schreiber, H. P. Nair, L. Miao, J. K. Kawasaki, J. N. Nelson, B. D. Faeth, Y. Lee, B. H. Goodge, B. Pamuk, C. J. Fennie, L. F. Kourkoutis, D. G. Schlom, K. M. Shen, *Nat. Commun.* **2021**, *12*, 59.
[67] X. Yang, Y. Wang, X. Tong, N. Yang, *Adv. Energy Mater.* **2022**, *12*, 2102261.
[68] Y. M. Ding, N. W. Li, S. Yuan, L. Yu, *Chem. Asian J.* **2022**, *17*, e202200178.
[69] P. Xiong, F. Zhang, X. Zhang, S. Wang, H. Liu, B. Sun, J. Zhang, Y. Sun, R. Ma, Y. Bando, C. Zhou, Z. Liu, T. Sasaki, G. Wang, *Nat. Commun.* **2020**, *11*, 3297.

[70] T. Zhang, Y. Liu, J. Yu, Q. Ye, L. Yang, Y. Li, H. J. Fan, *Adv. Mater.* **2022**, *34*, 2202195.
[71] G. Wu, X. Han, J. Cai, P. Yin, P. Cui, X. Zheng, H. Li, C. Chen, G. Wang, X. Hong, *Nat. Commun.* **2022**, *13*, 4200.
[72] B. Akgenc, A. Mogulkoc, E. Durgun, *J. Appl. Phys.* **2020**, *127*, 084302.
[73] M. Baskurt, I. Eren, M. Yagmurcukardes, H. Sahin, *Appl. Surf. Sci.* **2020**, *508*, 144937.
[74] J. Cenker, S. Sivakumar, K. Xie, A. Miller, P. Thijssen, Z. Liu, A. Dismukes, J. Fonseca, E. Anderson, X. Zhu, X. Roy, D. Xiao, J.-H. Chu, T. Cao, X. Xu, *Nat. Nanotechnol.* **2022**, *17*, 256.
[75] K. Chen, J. Deng, Y. Yan, Q. Shi, T. Chang, X. Ding, J. Sun, S. Yang, J. Z. Liu, *npj Comput. Mater.* **2021**, *7*, 79.
[76] O. T. Fauth, L. I. Bendavid, *J. Electron. Mater.* **2022**, *51*, 1358.
[77] L. Hu, J. Zhou, Z. Hou, W. Su, B. Yang, L. Li, M. Yan, *Mater. Horiz.* **2021**, *8*, 3306.
[78] X. Hu, Y. Zhao, X. Shen, A. V. Krasheninnikov, Z. Chen, L. Sun, *ACS Appl. Mater. Interfaces* **2020**, *12*, 26367.
[79] C.-C. Hsu, M. L. Teague, J.-Q. Wang, N.-C. Yeh, *Sci. Adv.* **2020**, *6*, eaat9488.
[80] H. Idzuchi, A. E. Llacsahuanga Allcca, X. C. Pan, K. Tanigaki, Y. P. Chen, *Appl. Phys. Lett.* **2019**, *115*, 232403.
[81] T. Li, S. Jiang, N. Sivadas, Z. Wang, Y. Xu, D. Weber, J. E. Goldberger, K. Watanabe, T. Taniguchi, C. J. Fennie, K. Fai Mak, J. Shan, *Nat. Mater.* **2019**, *18*, 1303.
[82] N. Miao, Z. Sun, *WIREs Comput. Mol. Sci.* **2022**, *12*, e1545.
[83] C. Moulsdale, A. Knothe, V. Fal'ko, *Phys. Rev. B* **2020**, *101*, 85118.
[84] M. Pizzochero, O. V. Yazyev, *J. Phys. Chem. C* **2020**, *124*, 7585.
[85] G. R. Portugal, J. T. Arantes, *J. Mater. Res.* **2022**, *37*, 490.
[86] M. Šiškins, M. Lee, S. Mañas-Valero, E. Coronado, Y. M. Blanter, H. S. J. Van Der Zant, P. G. Steeneken, *Nat. Commun.* **2020**, *11*, 2698.
[87] B. Sohn, J. R. Kim, C. H. Kim, S. Lee, S. Hahn, Y. Kim, S. Huh, D. Kim, Y. Kim, W. Kyung, M. Kim, M. Kim, T. W. Noh, C. Kim, *Nat. Commun.* **2021**, *12*, 6171.
[88] T. Song, M. W.-Y. Tu, C. Carnahan, X. Cai, T. Taniguchi, K. Watanabe, M. A. Mcguire, D. H. Cobden, D. Xiao, W. Yao, X. Xu, *Nano Lett.* **2019**, *19*, 915.
[89] F. Subhan, J. Hong, *J. Phys.: Condens. Matter* **2020**, *32*, 245803.
[90] Qi Wang, Z. Zhang, H. Huang, X. Song, Y. Bu, *Phys. Chem. Chem. Phys.* **2022**, *24*, 3834.
[91] Z. Wu, J. Yu, S. Yuan, *Phys. Chem. Chem. Phys.* **2019**, *21*, 7750.
[92] Bo Xu, S. Li, K. Jiang, J. Yin, Z. Liu, Y. Cheng, W. Zhong, *Appl. Phys. Lett.* **2020**, *116*, 052403.
[93] Y. Yue, B. Wang, N. Miao, C. Jiang, H. Lu, B. Zhang, Y. Wu, J. Ren, M. Wang, *Ceram. Int.* **2021**, *47*, 2367.
[94] J.-M. Zhang, Y.-Z. Nie, Xi-G Wang, Q.-L. Xia, G.-H. Guo, *J. Magn. Magn. Mater.* **2021**, *525*, 167687.
[95] D. Zhong, K. L. Seyler, X. Linpeng, N. P. Wilson, T. Taniguchi, K. Watanabe, M. A. Mcguire, K.-M. C. Fu, Di Xiao, W. Yao, X. Xu, *Nat. Nanotechnol.* **2020**, *15*, 187.
[96] J. Zhong, M. Wang, T. Liu, Y. Zhao, X. Xu, S. Zhou, J. Han, L. Gan, T. Zhai, *Nano Res.* **2022**, *15*, 1254.
[97] J. Zhou, X. Song, J. Chai, N. L. M. Wong, X. Xu, Y. Jiang, Y. P. Feng, M. Yang, S. Wang, *J. Alloys Compd.* **2022**, *893*, 162223.
[98] B. Chen, N. Gauquelin, N. Strkalj, S. Huang, U. Halisdemir, M. D. Nguyen, D. Jannis, M. F. Sarott, F. Eltes, S. Abel, M. Spreitzer, M. Fiebig, M. Trassin, J. Fompeyrine, J. Verbeeck, M. Huijben, G. Rijnders, G. Koster, *Nat. Commun.* **2022**, *13*, 265.
[99] H. Tabata, T. Kawai, *IEICE Trans. Electron.* **1997**, *80*, 918.
[100] C. Thiele, K. Dörr, S. Fähler, L. Schultz, D. C. Meyer, A. A. Levin, P. Paufler, *Appl. Phys. Lett.* **2005**, *87*, 262502.
[101] Y. Qi, L. Wang, Y. Jiang, Z. Wu, L. Wang, J. Gao, *Vacuum* **2017**, *135*, 13.
[102] M. Zheng, P. Guan, Y. Qi, Z. Tang, H. Ni, J. Gao, *Adv. Electron. Mater.* **2021**, *7*, 2100603.
[103] D. E. Shai, C. Adamo, D. W. Shen, C. M. Brooks, J. W. Harter, E. J. Monkman, B. Burganov, D. G. Schlom, K. M. Shen, *Phys. Rev. Lett.* **2013**, *110*, 87004.
[104] T. M. Riseman, P. G. Kealey, E. M. Forgan, A. P. Mackenzie, L. M. Galvin, A. W. Tyler, S. L. Lee, C. Ager, D. M. Paul, C. M. Aegerter, R. Cubitt, Z. Q. Mao, T. Akima, Y. Maeno, *Nature* **1998**, *396*, 242.
[105] A. P. Mackenzie, Y. Maeno, *Rev. Mod. Phys.* **2003**, *75*, 657.
[106] K. D. Nelson, Z. Q. Mao, Y. Maeno, Y. Liu, *Science* **2004**, *306*, 1151.
[107] A. N. Petsch, M. Zhu, M. Enderle, Z. Q. Mao, Y. Maeno, I. I. Mazin, S. M. Hayden, *Phys. Rev. Lett.* **2020**, *125*, 217004.
[108] V. Grinenko, S. Ghosh, R. Sarkar, J.-C. Orain, A. Nikitin, M. Elender, D. Das, Z. Guguchia, F. Brückner, M. E. Barber, J. Park, N. Kikugawa, D. A. Sokolov, J. S. Bobowski, T. Miyoshi, Y. Maeno, A. P. Mackenzie, H. Luetkens, C. W. Hicks, H.-H. Klauss, *Nat. Phys.* **2021**, *17*, 748.
[109] A. Herklotz, M. Kataja, K. Nenkov, M. D. Biegalski, H.-M. Christen, C. Deneke, L. Schultz, K. Dörr, *Phys. Rev. B* **2013**, *88*, 144412.
[110] W. P. Zhou, Q. Li, Y. Q. Xiong, Q. M. Zhang, D. H. Wang, Q. Q. Cao, L. Y. Lv, Y. W. Du, *Sci. Rep.* **2014**, *4*, 6991.
[111] S. Ren, Q. Tan, J. Zhang, *J. Semicond.* **2019**, *40*, 071903.
[112] M. Toth, I. Aharonovich, *Annu. Rev. Phys. Chem.* **2019**, *70*, 123.
[113] S. I. Azzam, K. Parto, G. Moody, *Appl. Phys. Lett.* **2021**, *118*, 240502.
[114] M. Kianinia, Z.-Q. Xu, M. Toth, I. Aharonovich, *Appl. Phys. Rev.* **2022**, *9*, 011306.
[115] J.-P. So, H.-R. Kim, H. Baek, K.-Y. Jeong, H.-C. Lee, W. Huh, Y. S. Kim, K. Watanabe, T. Taniguchi, J. Kim, C.-H. Lee, H.-G. Park, *Sci. Adv.* **2021**, *7*, eabj3176.
[116] K. Parto, S. I. Azzam, K. Banerjee, G. Moody, *Nat. Commun.* **2021**, *12*, 3585.
[117] A. Mukherjee, C. Chakraborty, L. Qiu, A. N. Vamivakas, *AIP Adv.* **2020**, *10*, 075310.
[118] X. Xu, Z. O. Martin, D. Sychev, A. S. Lagutchev, Y. P. Chen, T. Taniguchi, K. Watanabe, V. M. Shalaev, A. Boltasseva, *Nano Lett.* **2021**, *21*, 8182.
[119] C. Chakraborty, A. Mukherjee, H. Moon, K. Konthasinghe, L. Qiu, W. Hou, T. Peña, C. Watson, S. M. Wu, D. Englund, N. Vamivakas, *Optica* **2020**, *7*, 580.
[120] M. Yang, W. Gao, Q. Song, Y. Zhou, L. Huang, Z. Zheng, Y. Zhao, J. Yao, J. Li, *Adv. Opt. Mater.* **2021**, *9*, 2100450.
[121] Y. Zhao, F. Guo, R. Ding, W. F. Io, S. Pang, W. Wu, J. Hao, *Adv. Opt. Mater.* **2021**, *9*, 2100864.
[122] R. Ding, Y. Lyu, Z. Wu, F. Guo, W. F. Io, S. Pang, Y. Zhao, J. Mao, M. Wong, J. Hao, *Adv. Mater.* **2021**, *33*, 2101263.
[123] A. De Sanctis, I. Amit, S. P. Hepplestone, M. F. Craciun, S. Russo, *Nat. Commun.* **2018**, *9*, 1652.
[124] M. Zheng, H. Ni, W. Huang, Y. Qi, J. Zeng, J. Gao, *Appl. Phys. Lett.* **2017**, *111*, 172901.
[125] S. Bellani, A. Bartolotta, A. Agresti, G. Calogero, G. Grancini, A. Di Carlo, E. Kymakis, F. Bonaccorso, *Chem. Soc. Rev.* **2021**, *50*, 11870.
[126] L. Bastonero, G. Cicero, M. Palummo, M. Re Fiorentin, *ACS Appl. Mater. Interfaces* **2021**, *13*, 43615.
[127] J. Jiang, Y. Wen, H. Wang, L. Yin, R. Cheng, C. Liu, L. Feng, J. He, *Adv. Electron. Mater.* **2021**, *7*, 2001125.
[128] D. Liu, D. Luo, A. N. Iqbal, K. W. P. Orr, T. A. S. Doherty, Z.-H. Lu, S. D. Stranks, W. Zhang, *Nat. Mater.* **2021**, *20*, 1337.
[129] L. Gu, D. Li, L. Chao, H. Dong, W. Hui, T. Niu, C. Ran, Y. Xia, L. Song, Y. Chen, W. Huang, *Sol. RRL* **2021**, *5*, 2000672.
[130] Y. Mao, C. Qin, J. Wang, J. Yuan, *Phys. Chem. Chem. Phys.* **2022**, *24*, 16058.

[131] S. J. Kim, D. Kim, B. K. Min, Y. Yi, S. Mondal, V. T. Nguyen, J. Hwang, D. Suh, K. Cho, C. G. Choi, *Adv. Opt. Mater.* **2021**, *9*, 2101310.
[132] X. Jiang, W. Xie, X. Xu, Q. Gao, D. Li, B. Cui, D. Liu, F. Qu, *Nanoscale* **2022**, *14*, 7292.
[133] J. Jiang, Z. Chen, Y. Hu, Y. Xiang, L. Zhang, Y. Wang, G.-C. Wang, J. Shi, *Nat. Nanotechnol.* **2021**, *16*, 894.
[134] Q. H. Wang, A. Bedoya-Pinto, M. Blei, A. H. Dismukes, A. Hamo, S. Jenkins, M. Koperski, Y. Liu, Q.-C. Sun, E. J. Telford, H. H. Kim, M. Augustin, U. Vool, J.-X. Yin, L. H. Li, A. Falin, C. R. Dean, F. Casanova, R. F. L. Evans, M. Chshiev, A. Mishchenko, C. Petrovic, R. He, L. Zhao, A. W. Tsen, B. D. Gerardot, M. Brotons-Gisbert, Z. Guguchia, X. Roy, S. Tongay, et al., *ACS Nano* **2022**, *16*, 6960.

Yaping Qi is a Postdoctoral Researcher at Macau University of Science and Technology. She obtained Ph.D. degree in physics in 2019 at the University of Hong Kong. She was a Research Fellow in Prof. David A. Weitz's group at Harvard University from 2017 to 2018 and Research Associate at Purdue University from 2019 to 2021. She was a visiting postdoc at Aarhus University, Denmark from October to December 2021, and in the Department of Physics and Astronomy, the University of British Columbia in Canada from January to March 2022. She is currently working on 2D materials, thin films, and AI.

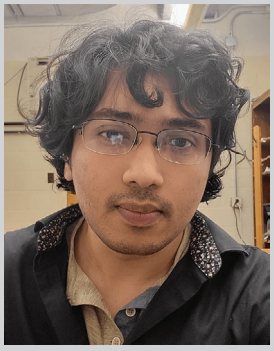

Mohammad A. Sadi is a Ph.D. candidate in Prof. Chen's group in the Elmore Family School of Electrical and Computer Engineering at Purdue University. He obtained his B.Eng. degree from National University of Singapore. His current focus is on strain engineering of 2D materials and studying their optical and transport properties.

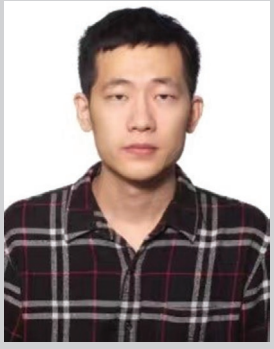

Yucheng Jiang is an associate professor at Jiangsu University of Science and Technology. He obtained his bachelor's degree at Nanjing University in 2010 and his Ph.D. degree in physics at the University of Hong Kong in 2014. He was a Research Assistant at the University of Hong Kong from December 2014 to October 2015. He joined Jiangsu University of Science and Technology as an Assistant Professor in March 2016. His group focuses on the discovery of 2D materials, thin films, and low-dimensional heterojunctions with novel optical, electrical, and magnetic properties.

Yong P. Chen is Karl Lark-Horovitz Professorof Physics and Astronomy and Professor of Electrical and Computer Engineering, Director of Purdue Quantum Science and Engineering Institute at Purdue University. He is also Villum Investigator and Professor at Aarhus University (Demark) and Principal Investigator in WPI (World Premier International Research Center)-AIMR (Advanced Institute for Materials Research) at Tohoku University (Japan) and MUST Chair Professor at Macau University of Science and Technology. He received his M.Sc. at MIT and Ph.D. at Princeton University. His research interests include nano/solid-state physics (graphene & 2D materials, topological insulators) and atomic/molecular physics (Bose–Einstein condensates, polar molecules).